The Role of TRP Channels in Auditory Transduction and Amplification in Drosophila

The role of TRP channels in auditory transduction and amplification in *Drosophila*

A dissertation presented

by

Brendan Peltonen Lehnert

to

The Division of Medical Sciences

in partial fulfillment of the requirements

for the degree of

Doctor of Philosophy

In the subject of

Neurobiology

Harvard University

Cambridge, Massaschusetts

April 2012

Dissertation Advisor: Professor Rachel I Wilson Brendan Peltonen Lehnert

The role of TRP channels in auditory transduction and amplification in *Drosophila*

Abstract

Auditory receptor cells rely on force-gated channels to transform sound stimuli into neural activity. These primary auditory neurons form the first stage of the neural circuits that support a host of higher-order functions, such as the localization of sound or the comprehension of speech. The mechanisms of sound transduction, as well as higher-order processes such as acoustic communication during courtship, can be studied in the fruit fly *Drosophila melangogaster*, a model organism with a suite of powerful genetic tools. However, this work is hampered by incomplete knowledge of the components of the *Drosophila* auditory system and a lack of high resolution techniques for investigating their function.

We used several approaches to identify candidate *Drosophila* central auditory neurons and developed techniques for measuring the activity of identified neurons *in vivo*. As an outgrowth of this work, we also developed a non-invasive method for measuring generator currents in the primary auditory neurons. Chapter 4 describes this technique and provides a basic characterization of the sensitivity of the *Drosophila* auditory system to sound. Determining the sensitivity of the *Drosophila* auditory system is necessary for understanding the neural basis of acoustic communication and has implications for the mechanism of transduction.

The force-gated ion channel that transforms sound into an electrical signal has not been identified in any species. Several TRP channels have been implicated in *Drosophila* auditory transduction, but mechanistic studies have been hampered by the inability to record subthreshold signals from auditory receptor neurons. We recorded generator currents from primary auditory neurons to assess the roles of several TRP family members in transduction. We found that the TRPN family member NompC is not required for transduction, despite the fact that it is required for the active amplification of motion by the auditory organ. Instead, NompC is required for a process that sensitizes the transduction complex to movement and regulates the resting forces on the complex. In contrast, the TRPV channels Nanchung and Inactive are required for responses to sound, suggesting they are components of the transduction complex. Thus, transduction and active amplification are genetically separable processes in the *Drosophila* auditory system.

Table of Contents

List of Figures

List of Tables

Acknowledgements

This work would not have been possible without the support and guidance of my advisor, Dr. Rachel Wilson. Rachel cares deeply for the members of her lab, manages her lab thoughtfully, and leads us by her example. My happiest moments in the lab have been when Rachel and I have worked together at the rig. I am tremendously grateful for the opportunity to learn from her and know that I will miss her advice and good company.

Rachel fills her lab with modest, talented people who share her passion for science. I would like to thank my colleagues Joe Bell, Vikas Bhandawat, Mehmet Fisek, Quentin Gaudry, Nathan Gouwens, Betty Hong, Hokto Kazama, Wendy Liu, Shaw Olsen, Katherine Nagel, Willie Tobin, Emre Yaksi, and Zhou (Joey) Yi for helping me to grow as a person and as a scientist.

I am very grateful for the training provided by my first mentor at Stanford University, Tom Middendorf. I am also grateful to his colleague, Weiyan Li, who patiently taught me the patch clamp recording technique.

I found that the Program in Neuroscience and the Department of Neurobiology provided an exciting and supportive environment. David Corey, Gary Yellen, Bernardo Sabatini, and John Assad served on my Dissertation Advisory Committee and provided excellent feedback as my work progressed. John and Bernardo both encouraged me to develop a method for applying a non-zero-mean stimulus to the antenna. Gary provided the insight concerning setpoint jitter that is included in our model of transduction. Finally, David routinely provided technical assistance and advice in excess of his committee obligations. I must also thank Wade Regehr and Mike Myoga for making me part of their synaptic physiology journal club early in my graduate career. Mark Andermann, Aaron Kerlin, and Vincent Bonin in the Reid lab provided useful assistance during the construction of the two photon microscope. Tim LaFratta and John Leblanc machined a great deal of my equipment.

I must express my gratitude to the National Science Foundation and the Sault Ste. Marie Tribe of Chippewa Indians for supporting my graduate work.

I must thank parents and brother for their love and support, which was remarkably constant throughout all twelve of my father's Marine Corps duty stations. Finally, I am deeply grateful to my wife and fellow PIN student Lulu Wang, whose good judgment and good cheer has made all my labors light.

Chapter 1

Introduction

We experience the world through our senses, which guide movement and inform decisions. A fundamental goal in neurobiology is to understand the mechanisms by which the physical world is transduced by primary sensory neurons.

Mechanosensation is vital to all living organisms, and an enormous diversity of mechanosensitive cell types are found in nature. Examples include the specialized hair cells of the inner ear that are dedicated to the perception of sound, as well as single celled bacteria whose mechanosensitive channels allow them to survive when faced with an osmotic challenge (Kung, 2005). We rely on mechanotransduction for our familiar senses of hearing, balance, proprioception, and visceral sensation, but also for homeostatic functions, as mechanosensitive cells report mechanical forces acting on bladder, kidney, and arteries. Despite the tremendous latitude of roles performed by biological mechanosensors, the molecular identity of the channels that convert force into electrical current has been largely a matter of conjecture. Moreover, the molecular and cellular mechanisms that modulate the forces acting on these mechanosensitive channels are also poorly understood.

1.1 *Drosophila*: A model organism for the study of mechanosensation

The molecular identities of mechanically-gated channels and the accessory proteins essential for their function are for the large part elusive, with some notable exceptions. In 1994, Ching Kung and colleagues identified the bacterial ion channel MscL after biochemical isolation of the channel protein and direct sequencing of its N-terminal residues (Sukharev et al., 1994). The success of this approach relied on the ability to activate MscL channels reconstituted into liposomes with suction; Many native mechanosensitive conductances require delicate, specialized mechanical structures for their activation (for example, the hair cell tip-link), and thus are not amenable to this approach.

Drosophila is a model organism that is well-suited to the study of mechanotransduction, as it has been used to identify candidate genes that might encode essential elements of the mechanotransduction complex, as well as to validate candidate mechanotransducers identified in other systems. In Drosophila, the components of mechanosensors have been identified through forward genetic screens for behavioral deficits or candidate approaches that take advantage of the ease of genetic manipulation in this model organism.

Mechanosensitive neuron types

Drosophila have two major classes of mechanosensors: type I, non-ciliated neurons, and type II, ciliated neurons (Kernan, 2007). They are distuinguished by their dendritic anatomy and their requirement for supporting cells for proper transduction. Type I mechanosensors include external bristles that respond when deflected, campiform sensilla in the haltiers and wings that

are used for balance during flight, and the chordotonal organs in the antenna and appendages that mediate hearing and proprioception. All of these mechanosensors rely of supporting cells for their function, and these cells transmit force as well as maintain the ionic environment surrounding the sensory cilia. Type II neurons are multidendritic, innervate the body wall and internal viscera, and detect heat and noxious mechanical stimuli (Tracey et al., 2003).

Forward genetic screens identify mechanosensor components

Genetic manipulations that disrupt the function of the mechanosensitive neurons result in behavioral defects. Drosophila exhibit a catalog of behaviors that rely on mechanosensation, and defects in these behaviors have been used as the basis for forward genetic screens designed to uncover elements of the mechanotransduction complex. Defects in genes required for mechanosensation lead to a variety of phenotypes in the adult, such as uncoordinated movement, loss of negative geotaxis, reduced grooming behavior, failure to eclose from the pupal case, and a disinclination to initiate movement. Larvae exhibit stereotyped behavioral responses to gentle (defined as < 30 mN) and harsh (>30 mN) touch, and loss of sensitivity to these stimuli has been used to identify components of mechanotransduces (Kernan et al., 1994; Kim et al., 2012; Zhong et al., 2010). An influential study used this approach to identify the TRPN channel NompC, as well as other proteins that were later shown to be important for specifying proper development of chordotonal stretch receptors (Kernan et al., 1994). With slight modification, behavioral screens can also be used to identify *central neurons* implicated in processing mechanical stimuli (Armstrong et al., 2006).

Ion channels implicated in *Drosophila* mechanotransduction

The TRPN channel NompC and the TRPV channels Nanchung and Inactive are expressed in type II mechanosensitive neurons, though they show only partially overlapping expression patterns across the different subtypes. NompC is expressed in the external bristles, the femoral chordotonal organs, and the Johnston's Organ Neurons (JONs) in the second antennal segment(Lee et al., 2010). An Inactive-GFP fusion protein localizes to the JONs and proprioceptive chordotonal organs, but is absent from bristles (Gong et al., 2004). Multiple lines of evidence support the idea that NompC has a key role in mechanotransduction. Loss of the *C. elegans* homolog eliminates force-gated receptor currents in mechanosensitive cephalic neurons, and amino acid substitutions in the putative pore domain of the *C. elegans* channel can alter the ionic sensitivity of receptor currents (Kang et al., 2010). TRPV mutants lack auditory-evoked field potentials in the antennal nerve (Kim et al., 2003).

The ion channels Painless, Pickpocket, and Piezo are expressed in type I mechanosensitive neurons and all separately required for normal responses to noxious mechanical stimuli in larvae (Kim et al., 2012; Tracey et al., 2003; Zhong et al., 2010). It is important to note that these neurons are polymodal, and mediate larval responses to noxious thermal and light, as well as noxious mechanical stimuli (Tracey et al., 2003; Xiang et al., 2010).

Painless is considered to be a second member of the TRPN family that includes NompC, and its closest mammalian ortholog is ANKTM1, which has been shown to express in pain-sensing neurons in the dorsal root ganglion (Story et al., 2003; Tracey et al., 2003). Pickpocket is a Deg/Enac channel whose c. Elegans ortholog has been shown to be required for transduction of noxious mechanical force in an identified cephalic neuron (Geffeney et al., 2011). Piezo1 and

Piezo2 were identified in an RNAi-based screen for components of a mechanosensitive conductance in a neuroblastoma cell line (Coste et al., 2010). Of these three ion channels, only dmPiezo has been shown to be necessary for a mechanically-gated conductance in cultured *Drosophila ppk*-positive neurons (Kim et al., 2012). Dissection of the role of these various ion channels in the sensation of noxious mechanical awaits methods for performing *in vivo* recordings from *ppk*-positive neurons.

1.2 The antennal sound receiver

A mathematical description of the physical changes in the medium that comprise sound phenomena was first developed by John William Strutt Rayleigh, who extended Newton's Laws of Motion to a fluid continuum (Rayleigh, 1896). As a sound wave propagates, it produces changes in the pressure and velocity of particles in the medium. Pressure is a scalar quantity and the aspect of the sound field with which we are most familiar (due to the inherent pressure sensitivity of our hearing organs). Particle velocity is a vector quantity that takes into account the aggregate speed and direction of particles at a given point in space. Together, particle velocity and pressure form a complete description of the sound field. In free-field, far-field conditions (far away from the source of a sound and any objects that might alter the sound field), pressure and particle velocity are in phase and related to each other by the acoustic impedance of the medium. In other words, the region of the medium with the highest acoustic pressure is also where the particles that constitute the medium have the highest speeds in the direction of sound propagation.

The intensity of a sound stimulus is often expressed as the ratio of the root-mean square deviation from standard atmospheric pressure and the Standard Pressure Level. In the absence of sound, thermal fluctuations of particles in the medium define the ambient sound energy, which is specifies as 20 µPa (Standard Pressure Level) or 50 nm/s (Standard Velocity Level). At distances far away from the source of a sound, the magnitude of the sound pressure and the acoustic particle velocity falls off as the square of the distance. However, within about two wavelengths from the source of a sound, sound intensity does not obey this relationship, a phenomenon known as the near-field effect. The near-field effect is stronger for lower frequencies and results from the reactive behavior of the medium near the source. Additionally, the near-field effect has a more pronounced impact on the particle velocity of a sound than the corresponding pressure disturbance (Bennet-Clark, 1971). In the next section, I will discuss how Drosophila uses the near-field effect to facilitate acoustic communication.

The auditory systems of terrestrial mammals are pressure sensitive. This is a consequence of the structure of the hearing organ itself. The tympanic membrane forms a boundary between the atmosphere and the middle ear, and pressure equilibrates only slowly through the Eustachian tubes. Thus, the tympanal membrane moves in proportion to changes in the external atmospheric pressure. In contrast, the *Drosophila* auditory system is sensitive to the net velocity of air particles in the vicinity of the antenna (Kernan et al., 1994). The antennae of *Drosophila* are commonly divided into three segments based on their external anatomy. Attached to the 3rd antennal segment is the arista, a feather-like structure that extends laterally and is thought to act as a moment-arm that breaks the radial symmetry of the 3rd antennal segment (Gopfert and Robert, 2002a). The role of the arista is likely to be more nuanced, as aristal amputees show altered, not abolished sensitivity to sound (Schilcher, 1976).

Regardless, stimulation of the antenna with sound produces a rotation of the 3rd antennal segment relative to the 2nd antennal segment (Figure 1.1). The force produced by pressure gradient across the antenna is small relative to the force exerted by the bulk movement of air particles. Thus, antennal rotation is driven by the acoustic particle velocity much in the same way as wind acts on the sail of a boat.

The mechanics of the antenna's movement in response to a sinuisoidal input are well described by a damped-driven linear harmonic oscillator model, where the parameters of the model have an additional dependence on the intensity and frequency of the stimulation (Gopfert and Robert, 2002b). Fits of the power spectrum of the antenna's resting fluctuations estimate a quality factor of 1.1-1.4 and a resonant frequency in the range of 200-400 Hz (Gopfert and Robert, 2002b; Kamikouchi et al., 2009). The antenna mechanics show three features of an active process:

1) Spontaneous movement in the absence of a sound stimulus that exceeds estimates based on thermal fluctuations and entrains to a sound stimulus (Gopfert and Robert, 2003).

2) A compressive non-linearity that is absent at high frequencies and abolished in some mutants (Gopfert et al., 2006).

3) A phase *lead* relative to the particle velocity force (data not shown).

The degree of power gain associated with the active process declines from a factor of about 10 to 1 (no gain) as the sound intensity is increased.

Figure 1.1: The antenna rotates in response to sound.

(top) The schematic of the antenna shows the location of the laser measurement spots during sound stimulation. The second antennal segment is stationary during the stimulus. In contrast, measurements of the 3rd antennal segment show that it moves in response to the particle velocity stimulus. The medial and lateral edges of the third segment are moving in opposite directions, indicating a rotation.

(bottom) A method for quantifying sound-evoked antennal rotation. The sound-induced displacement of the antenna relative to the Laser Doppler Vibrometer is recorded at the lateral branch point. The length of the aristal lever is estimated by visual inspection. The angular displacement as a function of time is then calculated using the small angle approximation.

Figure 1.1 (continued): The antenna rotates in response to sound.

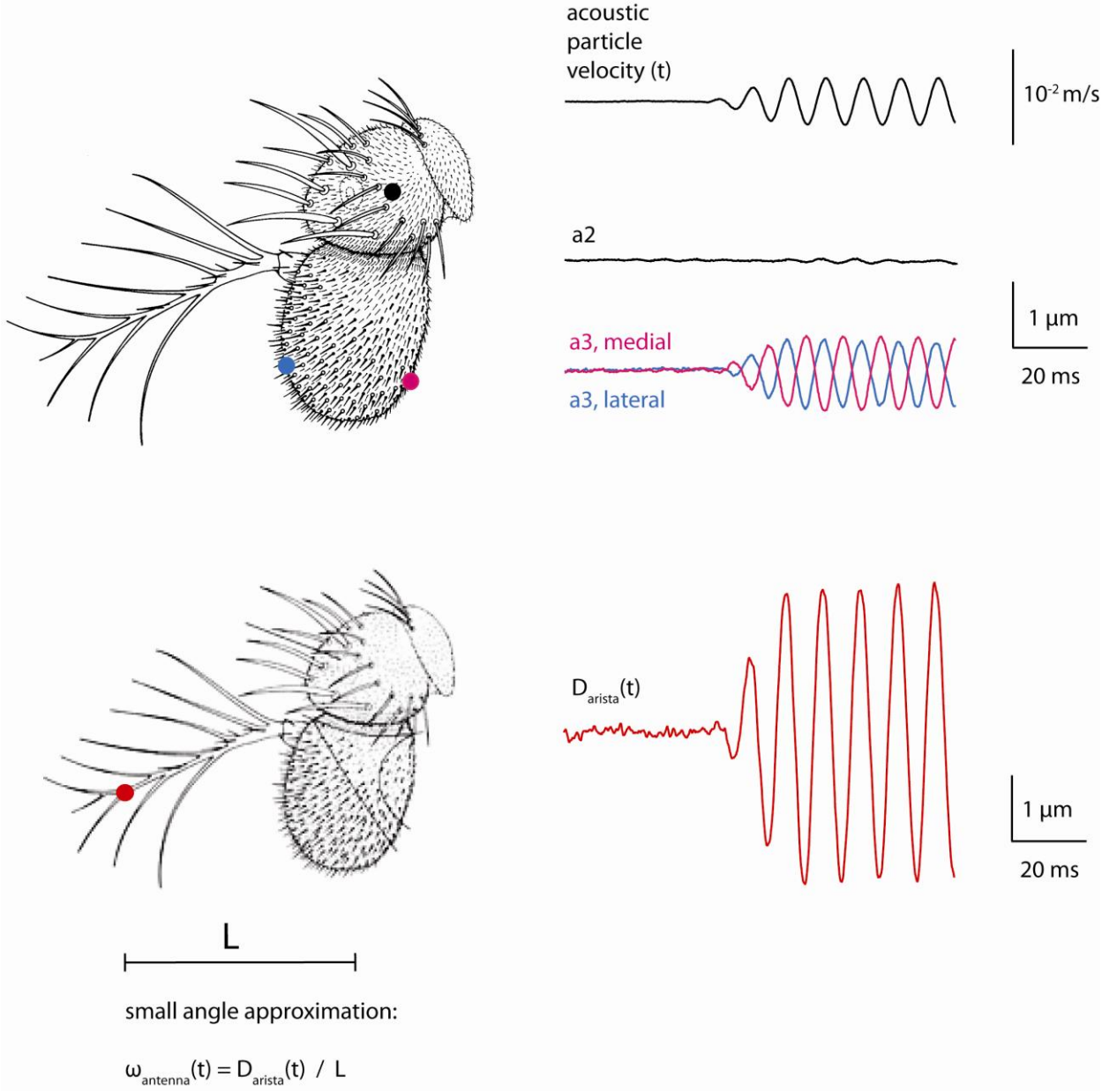

1.3 The anatomy of the *Drosophila* auditory system

Rotations of the antenna activate mechanosensitive neurons

Rotation of the 3rd antennal segment about its longitudinal axis is transmitted proximally by a "stalk" that ends in a hook-like structure in the 2nd antennal segment. The cell bodies of Johnston's Organ neurons (JONs), the primary auditory afferents, reside in the 2nd antennal segment as well (Eberl et al., 2000b). JONs are arrayed perpendicularly to the hook, and thus are thought to transduce acoustically-evoked movement of the antenna during the stretching and compression they experience as the hook sweeps out its arc (Gopfert and Robert, 2001).

JONs are organized into an estimated 227 scolopidial units, each containing 2-3 neurons (Boekhoff-Falk, 2007). JON axons project out of the antennae, joining the axons of olfactory receptor neurons (ORNS) to form the antennal nerve. Whereas ORNs terminate in the antennal lobe, JONs continue posteriorly to innvervate the Antennal Motor and Mechanosensory Center (AMMC) (Fig. 2a). There is a strong correspondence between the location of JON cell bodies within Johnston's Organ and their projection patterns in the AMMC. JONs have been classified on the basis of their specific project patterns into groups A,B,C,D, and E. The evidence that Group A/B JONs are acoustically responsive is that 1) though all JONs seem to respond to loud sounds, Group A/B has a lower threshold and 2) selective expression of tetanus toxin in Group B JONs abolishes song-evoked chaining behavior in males (Kamikouchi et. al., 2009). However, the GAL4 used to drive expression in the Group B JONs also bore an associated mutation (*yw*) known to impair courtship behavior(Drapeau et al., 2003). Group C/E JONs are thought to respond best to static deflections of the antenna, with Group C and E activated by medial and lateral deflections, respectively (Kamikouchi et al., 2009; Yorozu et al., 2009). At the beginning

of my thesis work, there were no identified central auditory neurons in *Drosophila*, and thus no indication of how these diverse JON signals were integrated in the brain.

1.4 Courtship and behavioral measures of sound threshold

In *Drosophila melanogaster*, courtship entails a series of stereotyped behaviors that begin when the male detects the female and (if successful) ends in copulation (Hall, 1994). While pursuing the female, males typically extend and vibrate one wing, generating a "love song" that favorably influences female sexual receptivity (Ewing, 1967; Rybak et al., 2002b). The song has a regular structure that is classically divided into distinct "sine song" and "pulse song" components (Fig. 4A). In *Drosophila melanogaster*¸ the sine song is approximately a 160 Hz tonal hum. The pulse song is a punctuated series of pulses separated by a mean inter-pulse interval (IPI) of 34 ms.

Courtship song stimulates mating

The ability of courtship song stimulation to enhance mating is generally assayed through playback experiments where the wings of males are removed (thus preventing sound production) and a speaker is used to deliver acoustic stimuli to populations of flies (Ewing, 1967; Kyriacou CP, 1982; Ritchie et al., 1999; Rybak et al., 2002b). Though not as spectacular or complex as the calls of other animals, the relative simplicity of the *Drosophila* courtship song lends itself well to parameterization, and these behavioral experiments are all conducted with synthetic song. The synthetic courtship song significantly decreases latency to mating. However, it should be

noted that this experimental design does not separate the effects of song on males vs. females (since both groups are exposed to song). Evidence that courtship song has an effect on mating that is *specific* to females comes from song prestimulation experiments. Decreased latency to mating was observed when *D. melanogaster* females were exposed to courtship song prior to mixing with males, relative to silent controls (Kyriacou and Hall, 1984; von Schilcher, 1976). Groups of male flies respond to courtship song with increased locomotor activity and by courting other males (Crossley et al., 1995), suggesting that song may also stimulate male courtship. Acoustic stimulation alone does not enhance *Drosophila* mating, as white-noise actually inhibits mating compared with silent controls.

Female preference for conspecific courtship song is thought to be a mechanism for maintaining sexual isolation between *Drosophila* species (Bennet-Clark and Ewing, 1969). Behavioral experiments have demonstrated that the sine song has a significant impact on female receptivity, but do not indicate that females discriminate between sine song (Kyriacou and Hall, 1984; Rybak et al., 2002a; von Schilcher, 1976). Additionally, behavioral evidence also suggests that the carrier frequency of the pulse song is not a major factor in song preference (Rybak et al., 2002a). Rather, the most important factor in promoting female receptivity seems to be the temporal structure of the pulse song. Specifically, females appear to be sensitive to the inter-pulse interval (IPI) that separates successive pulses (Bennet-Clark and Ewing, 1969; Kyriacou and Hall, 1984; Kyriacou CP, 1982; Ritchie et al., 1999).

Behavioral measures of sound threshold

Behavioral measures of auditory sensitivity based on male courtship behavior suggest that *Drosophila* have a comparatively high threshold for hearing, variously reported as 92 dB SPL (Schilcher, 1976) or ~72 dB SPL (Kamikouchi et al., 2009). This has led to the suggestion that the Drosophila hearing organ is strictly a near-field sound receptor, as courtship song only exceeds this threshold within a couple millimeters of the source (Bennet-Clark, 1971).

1.5 The role of Transient Receptor Potential (TRP) channels in auditory transduction

The TRPV channels Nanchung and Inactive and the TRPN channel NompC are expressed in primary auditory neurons, and mutant alleles of these genes alter transduction and antennal mechanics. Loss of NompC reduces sound-evoked electrical activity in the antennal nerve (Eberl et al., 2000a; Effertz et al., 2011). Additionally, knockdown of the zebrafish NompC homolog eliminates sound-evoked microphonic potentials in the lateral line organ, as well as behavioral responses to sound (Sidi et al., 2003). Moreover, loss of NompC abolishes the active amplification of sound-evoked antennal motion in *Drosophila* (Gopfert et al., 2006; Gopfert and Robert, 2003). Active amplification refers to a positive feedback process whereby motile elements in the primary auditory organ amplify sound-evoked motion. This phenotype is particularly interesting because active amplification also exists in vertebrate hair cells, and a component of active amplification is thought to depend directly on the gating of mechanotransduction channels (Hudspeth, 2008). Thus, by analogy, because the loss of NompC causes loss of active amplification, previous studies have inferred that NompC forms part of the transduction complex.

However, the putative selectivity filter of the NompC pore domain is not well-conserved in *Drosophila*, although it is highly conserved in the *C. elegans*, zebrafish, and *Xenopus* homologs (Kang et al., 2010). This raises the possibility that *Drosophila* NompC might not actually be a channel, or if it is, it might display different ionic selectivity. In addition, loss of NompC does not entirely eliminate sound-evoked field potentials in the *Drosophila* auditory nerve (Eberl et al., 2000a; Effertz et al., 2011), leading to the speculation that another gene might play a redundant function.

Two additional *Drosophila* TRP channels – Nanchung and Inactive – are also expressed in auditory receptor neurons (Gong et al., 2004; Kim et al., 2003), and likely function as a heteromer (Gong et al., 2004). These TRPV family members are not thought to be part of the transduction complex, because they localize to a subcellular region that is several microns away from the region occupied by NompC (Lee et al., 2010). Nevertheless, both Nanchung and Inactive are required for sound-evoked field potentials in the antennal nerve, which houses the axons of JONs (Gong et al., 2004; Kim et al., 2003). These potentials are thought to reflect mainly spike-mediated currents in JONs. Thus, it has been proposed that Nanchung and Inactive are required to amplify subthreshold electrical signals generated by the transduction complex, thereby producing signals large enough to elicit spikes in JONs (Gopfert et al., 2006; Lee et al., 2010; Nadrowski et al., 2008).

That said, it is not clear how Nanchung/Inactive might amplify a signal generated by the transduction complex. Amplification by second messengers is unlikely because these processes are much slower than the auditory transduction latency (Eberl et al., 2000a; Robert et al., 1996). Electrical amplification also seems unlikely, as Nanchung and Inactive form channels that are only weakly voltage-dependent in heterologous cells (Gong et al., 2004; Kim et al., 2003).

The roles of TRP channels in *Drosophila* auditory transduction have been difficult to resolve, due in part to the fact that recordings from individual auditory receptor neurons are not feasible. This is because JONs are very small cells embedded in a delicate antennal organ whose integrity is critical to their function.

1.6 Summary of the dissertation research

The results of this dissertation are described in three chapters. The first chapter details our strategy for identifying candidate central auditory neurons and provides basic characterization of two neuron types that were amenable to electrophysiological recording. We reasoned that identification of candidate central auditory neurons was a prerequisite for investigating the central representation of sound in *Drosophila*, but this work ultimately led to a novel method for measuring transduction in the primary auditory neurons.

The next two chapters contain the bulk of my dissertation work. Behavioral measures of the *Drosophila* sound threshold give the impression that their hearing is quite insensitive, while mechanical measurements of the hearing organ suggests that their hearing rivals our own. Chapter 2 addresses this conflict by describing the sensitivity of the *Drosophila* auditory system using a novel method for measuring auditory transduction. The work in Chapter 2 led us to question the prevailing model of transduction in *Drosophila*, and Chapter 3 investigates the mechanism by which the TRP channels Nanchung, Inactive, and NompC specify sensitivity to sound.

Chapter 2

General Methods

2.1 Electrophysiology

Recordings were made 6-18 hours post-eclosion because older flies showed substantially smaller sound-evoked currents as compared to flies <18 hours old. Currents were recorded from the Giant Fiber Neuron (GFN) *in vivo* using the whole-cell patch-clamp technique in voltage-clamp mode. Stable auditory responses from the GFN could be recorded for 1-4 hours. Flies were briefly cold anesthetized and immobilized using UV-curable adhesive in a hole cut into a piece of titanium foil within a larger flat recording platform. The upper side of the fly's head (above the platform) was bathed in oxygenated saline, while the underside of the head and both antennae (together with most of the thorax and all of the abdomen) remained dry. The posterior cuticle of the head was surgically removed to expose the posterior side of the brain, and the perineural sheath was removed with fine forceps. The preparation was then placed under an upright compound microscope equipped with an Hg arc lamp and a 40× water immersion objective (Olympus BX51). Prior to beginning a recording, the platform was oriented in a standard configuration with respect to the sound stimulus by rotating it until the fluorescently labeled GFN cell bodies were level in the field of view. After a stable whole-cell recording was obtained from the GFN under visual control, the microscope condenser was removed prior to sound stimulation to better mimic the sound field in the *in situ* particle velocity calibration.

The external saline solution was composed as previously described (Wilson et al., 2004b). The saline was recirculated continuously and was bubbled throughout the experiment with 95% O_2 / 5% CO_2. The internal pipette solution contained (in mM): 111 K-aspartate, 8 HEPES, 0.08 EGTA, 8 BAPTA, 3.2 MgATP, 0.4 Na_3GTP, 1.6 KCl, 10 biocytin hydrazide. The pH of the internal solution was adjusted to 7.3 with KOH and the osmolarity was adjusted to 265 mOsm. In the majority of experiments, the patch pipette was targeted to the GFN based on GFP visualization. In cases where labeling the GFN with GFP was difficult or undesirable, unlabeled GFNs were targeted based on their large nucleoli and cell body position, and biocytin fills were imaged *post hoc* to confirm that the recorded neuron was indeed the GFN.

Voltage-clamped currents were recorded from the GFN with an Axopatch 200B amplifier. The typical input resistance of the GFN was 50-100 MOhm, and estimates of access resistance based on the height of the fast current transient during test voltage steps were 8-20 MOhm. We saw no evidence of spiking, or indeed any active sodium conductance, in any of our GFN recordings. Pilot experiments comparing wild type flies and the *nan*^{36a} mutants showed little difference in the power spectra of recorded currents at frequencies above ~1.5 kHz, so all subsequent experiments were performed with the amplifier's internal four-pole Bessel filter set to a 2 kHz cutoff frequency. Data were digitized at 10 kHz by a 16 bit A/D converter (National Instruments, BNC-2090A) and acquired in Igor Pro (Wavemetrics).

To perform auditory field potential recordings from the antennal nerve, the fly was first immobilized with wax and UV-curable adhesive in the end of a trimmed 200-μL micropipette tip. The lateral face of the second antennal segment was glued to the head to stabilize the electrode insertion site. A saline-filled quartz recording electrode (30 - 50 MOhm resistance) was inserted in the joint between the first and second antennal segment from the dorsomedial side. A

pulled borosilicate glass capillary filled with saline was inserted into the eye to serve as a reference electrode. Field potentials were recorded using an Axopatch 200B amplifier (Axon Instruments) in I=0 mode, low-pass filtered at 2 kHz using the amplifier's internal four-pole Bessel filter, digitized at 10 kHz by a 16 bit A/D converter (National Instruments, BNC-2090A), and acquired in IgorPro (Wavemetrics). Measurements were performed on flies 12 – 48 hours post-eclosion.

2.2 Particle Velocity Microphone Calibration

The propagation of a sound wave is inextricably linked to changes in the pressure and the velocity of particles in the medium. Far away from a sound's source, the time-varying particle velocity component ( ) of a sound wave is in phase with the pressure component and is related to it through the acoustic impedance of the medium. For air at sea level and 20 degrees Celsius, the acoustic impedance is the product of the density of air (1.21 kg/m^3) and the speed of sound (340 m/s). Thus:

To calibrate our particle velocity microphone, we measured its ouput along with the output of a calibrated pressure microphone under conditions where we could infer particle velocity from pressure. We presented 1-second long pure tones at 7 frequencies and 4 intensities using a function generator driving an amplifier (Crown XLS202) and speaker (Morel SCM634). We

simultaneously acquired the voltage responses of two microphones. First, we used a pressure microphone (Brüel & Kjaer 4176, used with preamplifier type 2671-W-001). The voltage output of this microphone ( ) is related to the sound pressure ( ) by a sensitivity factor which is independent of frequency (equal to 49.4 mV/Pa, according to the manufacturer's specifications):

The particle velocity microphone (Knowles Electronics NR-23158) outputs a voltage that is related to the pressure gradient in space ($\partial p/\partial x$) by a sensitivity factor) that depends on frequency. This sensitivity factor of this microphone is what we want to measure. Measuring the pressure gradient allows us to compute the particle velocity (see below), which is the relevant feature of a sound stimulus for the *Drosophila* antenna.

The calibration was performed outside in a large grassy open space to minimize sound reflection. The two microphones were placed 4 meters away from the speaker, with the front face of the Knowles Electronics microphone perpendicular to the direction of sound propagation (Figure 2.1A).

Figure 2.1: Particle velocity microphone calibration and in situ measurements of particle velocity.

(A) Schematic illustrating the arrangement of the speaker and microphones.

(B) Integrated output of the pressure-gradient microphone plotted versus particle velocity (300 Hz tone).

(C) Sensitivity of the pressure-gradient microphone and its phase relationship to the pressure microphone.

(D) Particle velocity of all test stimuli used in this study. Points connected by a line represent tones having approximately equal particle velocities.

(E) Comparison between pressure and particle velocity, showing the near-field effect for low frequency stimuli.

Figure 2.1 (continued): Particle velocity microphone calibration and in situ measurements of particle velocity.

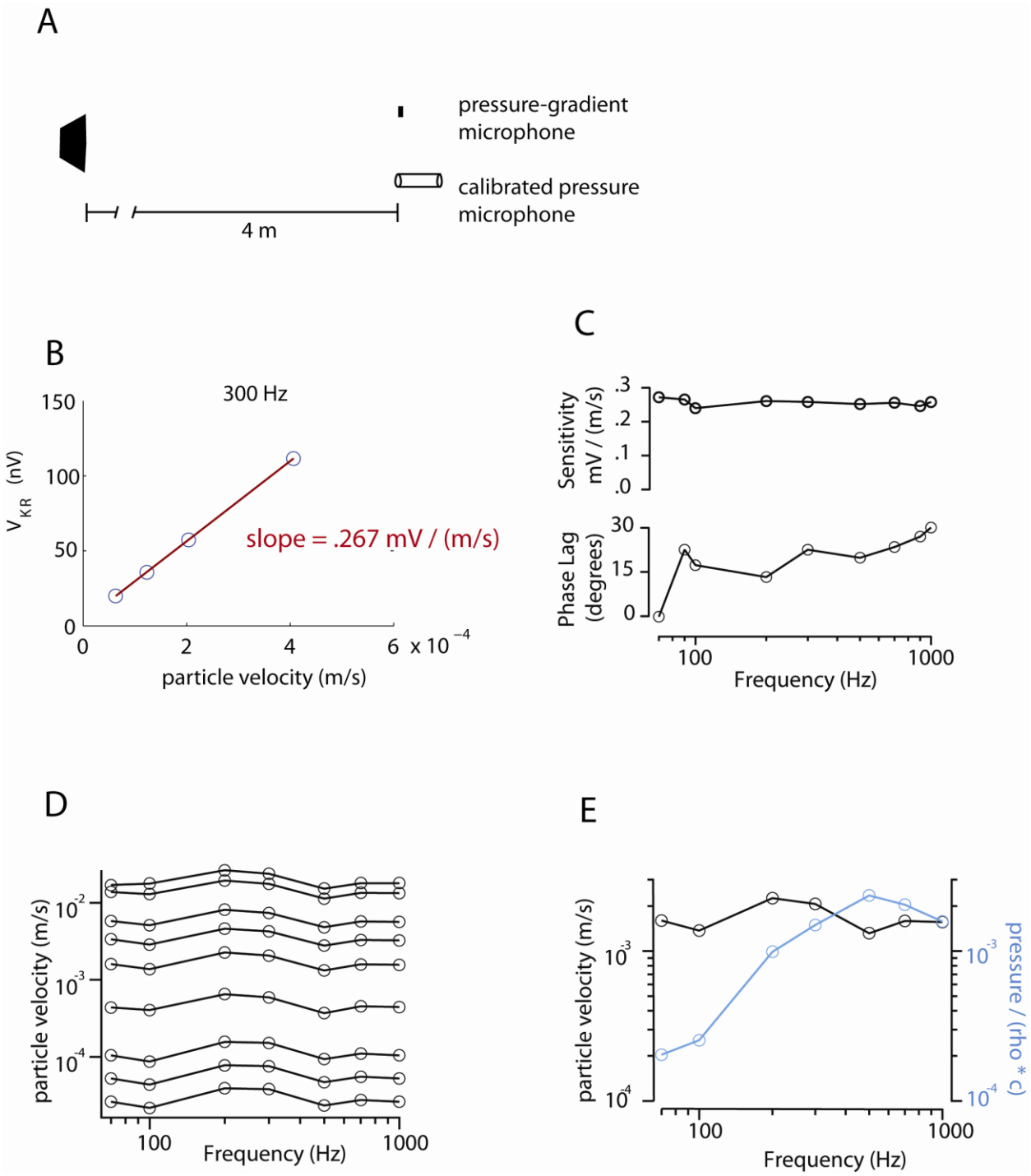

Recall that under far field conditions, the time-varying particle velocity component ( ) of a sound wave is in phase with the pressure component and is related to it through the density of air (1.21 kg/m^3) and the speed of sound (340 m/s):

Thus

The pressure gradient in space is related to gradient in time by the speed of sound:

And so

Integrating, we obtain

Recall that the voltage output of the Knowles Electronics microphone ( ) is proportional to $\partial p/\partial x$. We define a sensitivity factor ( ) which relates the time integral of to the particle velocity:

Integration of the signal was performed in software. For each test frequency, we measured the Fourier amplitude of the time integral of at that frequency, and also the Fourier amplitude of . Dividing the latter by and fitting a line gives us the slope (Figure 2.1B). The calibrated sensitivities of the microphone for all frequencies in our test set are shown in Figure 2.1C.

Figure 2.1C also shows the phase delays between the integrated signal and . To determine the phase of the particle velocity wave, we took account of these phase delays, plus the phase delay of the Brüel & Kjaer microphone and preamplifier (according to manufacturer's specifications).

During this calibration procedure, the output of both microphones was amplified and filtered (Stanford Research SR560, 6dB/octave bandpass with 1 Hz and 30kHz cutoffs) prior to digitization (Measurement Computing USB-1208FS). The relative time delay between digitization of the two channels was measured and subtracted from the second channel.

In order to generate several sets of tones where all the tones in a set have approximately the same particle velocity at the fly, we generated sound files where the amplitude of the voltage output for each tone was adjusted to achieve this. This adjustment is necessary because the output of the speaker is not necessarily flat with frequency, and because the intensity of high-frequency tones decays more rapidly with distance than the intensity of low-frequency tones. Supplementary Figure 2.1D shows that particle velocities for each frequency within a set were approximately equal, as measured with the Knowles Electronics (velocity) microphone at the position of the fly. Because the speaker was positioned differently for presentation to the right and left antenna, we created different sound files with slightly different amplitude adjustments for these two speaker positions. As expected, when we instead place the Brüel & Kjaer (pressure) microphone at the fly's position, we see a discrepancy between the output of the two microphones which depends

on frequency (Figure 2.1E). This reflects the frequency dependence of the near-field effect (Rayleigh, 1896).

2.3 Laser Doppler Vibrometry

Sound-driven antennal movements were measured using a laser Doppler vibrometer (Polytec OFV-5000 equipped with OFV-500, VD06, and DD-500 decoder boards). A calibrated particle velocity microphone was placed within 3 mm of the fly, such that the stimulus and mechanical response were simultaneously recorded and acquired in IgorPro. We removed the fly's legs and waxed the abdomen to a 200-μL micropipette tip having a shaved tip. UV-curable adhesive was used to fix the head to the body, and also to fix the second antennal segments to the head. The micropipette tip was mounted on a micromanipulator, and was visualized using a CCD video imaging system coupled to a 20× objective (Polytec OFV-534, Mitutoyo MP20×). Prior to sound stimulation, the fly was translated using the micromanipulator until the laser measurement spot coincided with the most distal branch point of the arista. Aristal displacements along the axis of measurement were converted into rotations by measuring the distance from the laser spot to the midline of the third antennal segment, and then taking the small angle approximation. We report rotation (rather than antennal displacement) because this measure should not depend on the position of the laser measurement spot on the arista. Flies were excluded from analysis of sound-induced antennal rotations if the free fluctuations of the antenna showed the higher frequency mechanical resonance and reduction in amplitude characteristic of dead flies.

2.4 Piezoelectric Antennal Displacement

A piezoelectric stack was fixed on a hollow titanium arm (McMaster-Carr) and mounted on a micromanipulator (MP-225, Sutter Instruments). Elastic lashing between the manipulator arm and microscope stage was used to shift the natural 70 Hz mechanical resonance of the mounted assembly to 400-600 Hz. Movement of the piezoelectric stack was transferred to the fly's antenna using a tungsten stimulus probe (#UEWLGGSE5N1J, World Precision Instruments). The tip of the probe was visualized using a custom-built imaging system (consisting of a miniature video camera and a 50× air objective) that was mounted in place of the condenser in the BX-51 microscope (i.e., under the titanium foil) after the whole-cell recording was obtained. To achieve a high contrast image of the arista and probe tip, the preparation was back-lit using the upright compound microscope's epifluorescence system. The probe tip was slowly maneuvered from a position below the fly into contact with the arista. In some experiments, we used a quick-drying two-component epoxy to attach the probe to the arista. In most experiments, however, we instead relied on an intrinsic electrostatic attraction between the probe and the arista. To facilitate a tight attachment, the probe tip was bent so as to increase the contact surface area with the arista. Step rotations were presented every 0.8 sec in a deterministic, pseudorandom order. Experiments were included in the data set if they contained at least 800 trials.

Piezoelectric commands were synthesized in software, delivered as an analog output at 10 kHz, and filtered with an 8-pole bessel filter (Frequency Devices LPF 900). A filter cutoff frequency of 3 kHz was chosen to stay within the specified operating limits of the high-current piezo amplifier (Physik Instrumente E-501, E-505). The amplifier drove a housed piezoelectric stack (P-810.30, 1 μF capacitance, 12 kHz unloaded resonance frequency, Physik Instrumente). Laser Doppler vibrometric measurements of the displacement of the piezoelectric stack showed a linear relationship to the applied voltage command with a scale factor of 474 nm/V. Hysteresis

was less than 10% of the commanded movement for the protocols employed in this study. For all step stimuli, the rise time (from 10% of maximum to 90% of maximum) as measured with the Laser Doppler vibrometer was 300 – 400 microseconds. The rotations produced by piezoelectric actuation of the antenna were calculated from laser Doppler vibrometric measurements of the motion of the stimulus probe.

2.5 Two Photon Microscopy Laser Scanning Microscopy

Zhou Yi and I constructed a two photon microscope laser scanning microscope (2PLSM) to enable PA-GFP neural tracings experiments and functional imaging deep in the neuropil. The 2PLSM was constructed around a commercially available Olympus BX-51 microscope. The excitation source was a tunable, ultra-fast Ti: sapphire laser (Mai Tai, Spectra Physics). The beam was expanded 6-fold using standard optics and projected onto a pair of galvanometric scan mirrors (6210H, 6mm, Cambridge Technology) situated inside a custom-built scanhead. The scanhead was inserted into the infinity space above the microscope objective between the objective holder and the epifluoresence turret and eye-pieces. Excitation light passing through the scanhead was further expanded by a telescope (200 mm Thor Labs AChromat, Olympus FV-PL-W3 pupil transfer lens). The lenses were situated such that the scan mirrors were optically conjugate to the back aperature of the objective, which was fully filled by the excitation light. Computer-directed rotations of the scan mirrors produced a translation of the diffraction limited focal spot in the sample plane, enabling imaging.

Epifluorescent and transfluorescent light was collected by an optical miniaturization system and bandpass filtered (FF01-534/30-50, Semrock) prior to detection by gallium arsenide

photo multiplier tubes (H7422P-40MOD, Hamamatsu). The MOD suffix refers to the absence of a cooling module that was removed to provide better access to the photocathode. Analog output from photo multipliers was amplified with a current preamplifer (SR570, Stanford Research Systems) then acquired via ScanImage (Pologruto et al., 2003) through a data acquisition board (PCI-6110, National Instruments).

For the PA-GFP photoactivation experiments, the brain was first mounted ventral-side-up on a poly-L-lysine coated coverslip. The AMMC was located via photoactivation of the antennal nerve of on the basis of the background fluorescence imaged at 910 nm. After focusing the laser selectively on the AMMC, the laser was tuned to 710nm and scanned over the photoactivation area four - ten times (128x128 pixels, 4ms/line) with an inter-scan interval of one minute to allow for diffusion of PA-GFP within the neuron. The subsequent photoactivated signal was then re-imaged at 925 nm.

2.6 Data Analysis

Unless otherwise noted, all analyses were performed in IgorPro (Wavemetrics). Spontaneous events (i.e., putative JON spikes) were detected with a shape template using an automated routine. The initial event template consisted of a single event, and was selected from a portion of the trace that was not included in the analysis. Events identified with this initial template were averaged, and this average was input into the detection routine for the final analysis. Recordings were excluded from the spontaneous event analysis if the amplitude of the unitary event was less than 65 pA, as it was difficult to accurately identify events in these cases. All generator currents displayed in the figures represent averages across many trials with the

same stimulus in the same cell, and measurements of generator currents were always performed on trial-averaged data. Trial-averaged generator currents were smoothed by convolving them with a 0.5-msec Gaussian prior to analysis or display in figures. The peak current evoked by a step stimulus was taken as the minimum or maximum in the 7 msec after step onset. The rise time of generator currents was calculated as the time elapsed between 10% of maximum and 90% of maximum. The Fast Fourier Transform (FFT) was used to calculate the antenna's displacement during a sound stimulus, the magnitude of the particle velocity sound stimulus, and the 1f and 2f signal in the frequency domain representation of generator currents. In Figure 5.7B, the decay in the total current (in the response to the 200 Hz tone) was calculated by comparing the peak current in a 30-msec window starting at sound onset, versus the peak current in a 10-msec window starting 70 msec after sound onset. In Figure 5.7C, the amplitude of phasic oscillations (in the response to the 100 Hz tone) was calculated by taking the FFT at either the 1f or 2f frequencies, whichever yielded the larger signal over the entire response. The decay in the amplitude of phasic oscillations was calculated by comparing a 20-msec window starting 28 msec after sound onset, versus a 20-msec window starting 150 msec after sound onset. In Figure 5.7D, the tail current (in response to the 200 Hz tone) was calculated as the mean current over a 10-msec window starting 30 msec after sound offset, and was expressed as percentage of the mean sound-evoked current over the entire unramped portion of the preceding tone.

Mean values with error bars in all figures represent averages across cells, and all error bars represent the SEM computed across cells. Statistical analysis was performed using either Matlab or R version 2.9.2 with the companion to applied regression package (obtained from http://www.r-project.org/). Fisher's F-test (with a $p>0.05$ criterion) was used to test for

homoskedasticity prior to any performing t-tests. If the two sample distributions were not homoskedastic, we performed Welch's two-sample t-test.

Chapter 3

Identification of candidate *Drosophila* central auditory neurons

3.1 Introduction

Many animals communicate using species-specific acoustic signals – female crickets recognize the temporal patterns of their conspecific song (Hoy, 1979), and zebra finches can recognize the call of their mate (Miller, 1979). A great deal is known about the acoustic structure of calls and their effect on animal behavior, yet far less is known about the neurobiological mechanisms that accomplish these recognition tasks. We reasoned that the *Drosophila* auditory system might serve as a model for understanding how neurons acquire tuning to specific temporal sequences of sounds. In contrast to the limited acoustic repertoire of other genetic model organisms, *Drosophila* produce elaborate songs during courtship. During courtship, *Drosophila* males produce a "love song" that increases female sexual receptivity (Bennet-Clark HC, 1967). This song is produced by beating wings and contains a regular series of pulses with a characteristic interpulse interval (IPI). The IPIs of courtship song differ across *Drosophila* species, and behavioral assays show that female flies can make exquisite distinctions between synthetic songs that differ only in their IPIs (Bennet-Clark HC, 1967; Ritchie MG, 1999).

As a model circuit, this system offers several advantages: powerful genetic tools, a sensory stimulus that is easily parameterized and manipulated, and clear behavioral relevance.

In particular, it has recently become possible to measure the activity of single neurons in the fly brain with patch-clamp electrophysiology (Wilson et al., 2004a). This technique allows the measurement of electrical signals within the primary neurons with sub-millisecond resolution, which is important given that acoustic stimuli fluctuate on fast timescales. However, at the outset of this work, none of the elements of this circuit – *Drosophila* central auditory neurons – had been identified. Thus, we pursued several approaches to identify such neurons.

Identification of candidate auditory neurons

There are no strong constraints on the location of the somata of central auditory neurons in the *Drosophila* brain: our search space was an estimated 100,000 neurons distributed over the approximately 300 μm × 300 μm × 700 μm volume of the brain (Wang et al., 2004). I took three approaches to identify central auditory neurons, all of which relied on the *a priori* expectations regarding their connectivity or anatomy. The first approach attempted to identify acoustically responsive neurons by expressing the genetically-encoded calcium indicator G-Camp throughout the fly brain. Stimulation of the primary auditory neurons may synaptically excite higher-order auditory neurons, which would then be identified through the subsequent increase in cytosolic calcium. The second approach used multiphoton PA-GFP neural tracing to identify neurons that had processes that overlapped with the axons of the primary auditory neurons. The third (and most successful) approach was conceptually similar and involved a visual screen of GAL4 lines for expression in the AMMC.

Functional Imaging

To functionally identify higher-order auditory neurons, we developed a preparation that allowed stimulation of the afferent nerve and optical measurements of any corresponding activity in postsynaptic central neurons. We excited the axons of the antennal nerve with a stimulus pipette while we visualized any resulting calcium signals in central cholinergic neurons. Electrical stimulation of the antennal nerve should activate olfactory receptor neurons and the JONs, as both type of axons traverse the nerve (Kamikouchi et al., 2006). We initially piloted this approach in the olfactory system, where the location of higher-order neurons is known (Figure 3.1 A).

As shown previously, stimulation of the primary olfactory neurons produces a G-CaMP signal in the cell bodies of olfactory projection neurons (Root et al., 2007)(Figure 3.1 C). The G-CaMP signal is abolished by the addition of the acetylcholine receptor antagonist mecamylamine, demonstrating that it required chemical synaptic transmission between the (first-order) olfactory receptor neuron and the (second-order) olfactory projection neuron. However, we were unable to identify central neurons that responded to antennal nerve stimulation outside of the olfactory antenna lobe using this technique. We can exclude the idea that electrical stimulation of the antennal nerve failed to stimulate JONs, because we saw G-CaMP signals when the expression of indicator was restricted to these neurons (Figure 3.1D).

Olfactory projection neurons lack active conductances in the soma (Nathan Gouwens and Brendan Lehnert, unpublished observations) and somatic G-CaMP signals are weaker than those in the neuropil (Root et al., 2007).

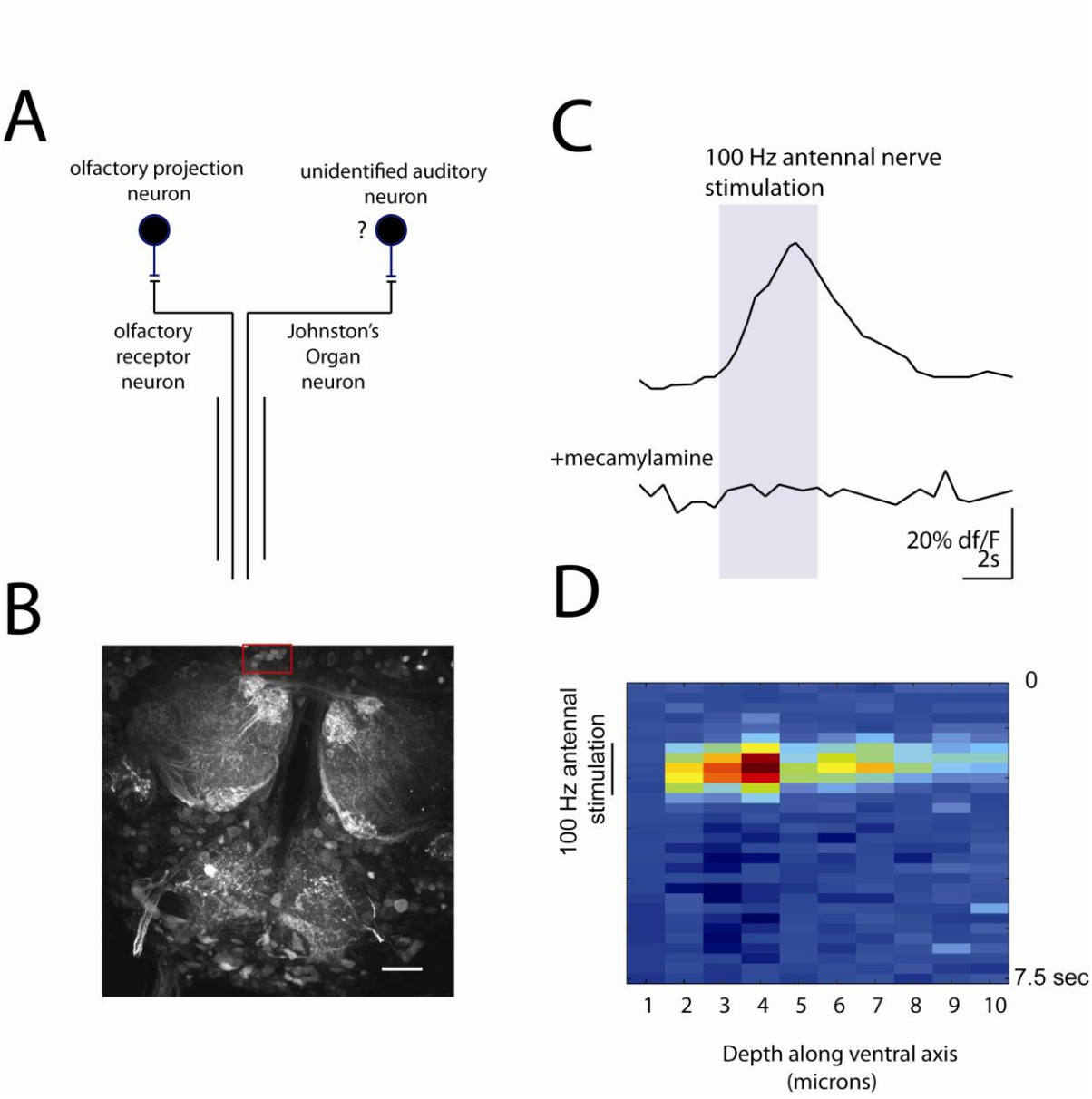

Figure 3.1: An approach to identifying second-order auditory neurons based on functional imaging.

(A) Schematic representation of the first and second order neurons of the olfactory and auditory system.

(B) A z-projection of a brain expressing G-CaMP in cholinergic neurons. The red box is the ROI.

(C) Stimulation of the antennal nerve produces a calcium signal that is abolished in mecamylamine.

(D) Stimulation of the antennal nerve produces a G-CaMP signal in JONs.

In the cricket omega-1-neurone (an auditory interneuron), acoustic stimulation elicits very weak somatic signals juxtaposed with large changes in indicator fluorescence in dendritic and axonal regions. Therefore, in some insect neurons, activity-evoked somatic calcium signals might reflect intracellular diffusion, not entry of calcium through somatic transmembrane ion channels. The lack of a local calcium entry in the cell bodies of central auditory neurons may explain our inability to identify them through increases in G-CaMP fluorescence.

Photactivatable Green Fluorescent Protein (PA-GFP) tracing

The elaborate processes of individual neurons can be visualized by several techniques, one of which involves intracellular injection and subsequent diffusion of a fluorescent dye (Stretton and Kravitz, 1968). Neural tracing with PA-GFP extends this approach by obviating the need for a patch pipette and by placing the tracing molecule under genetic control. PA-GFP is an engineered form of GFP which exhibits fluorescence at long wavelengths that greatly increases after photoconversion by shorter wavelength light (Schneider et al., 2005). Photoconversion and fluorescent imaging of PA-GFP is compatible with multiphoton imaging approaches, allowing selective photoconversion of small volumes and subsequent imaging of neural processes throughout the *Drosophila* brain. Previously, this technique had been used successfully to selectively label DA1 olfactory projection neurons and to discover novel elements of the fruitless-positive courtship circuit (Datta et al., 2008; Ruta et al., 2010).

The goal of these experiments was to identify putative second-order auditory neurons by photoactivating the neuropil volume where the JON axons terminated. We reasoned that this manipulation would also photoactivate PA-GFP in the dendrites of second-order neurons, which

would then diffuse and label cell bodies. The experiments were performed in flies expressing PA-GFP in all cholinergic neurons, the main class of excitatory neurons in the Drosophila brain.

Photoactivation was targeted to the AMMC either by first photoactivating the antennal nerve to visualize JON terminals in the AMMC or on the basis of resting fluorescence (Figure 3.2.A). Subsequent imaging of the entire brain with long wavelength light revealed photoactivated GFP in the AMMC, as well as diffusion of the activated fluorophore outside the photoactivated volume (Figure 3.2.B and C). The results of multiple experiments showed a preponderance of photoactivated cell bodies on the anterior surface of the brain, in the region directly ventral to the antennal nerve (Figure 3.2.D).

Despite the robustness of this finding, photoactivation of individual neuron cell bodies in the region identified in Figure 3.2.D did not illuminate processes that innervated the AMMC (data not shown). Genetically identified neurons in *Drosophila* and functionally-defined neurons in other invertebrates show strong stereotypy between animals in their projections in the neuropil (Pfeiffer et al., 2008; Stretton and Kravitz, 1968). However, the relative position of the cell body is far more variable, and this observation may be related to our inability to identify the same cells from preparation to preparation. The "hot-spot" identified through this technique corresponds to the cell body location of the B1 neurons (see next section), but it did not reliably label candidate second-order auditory neurons.

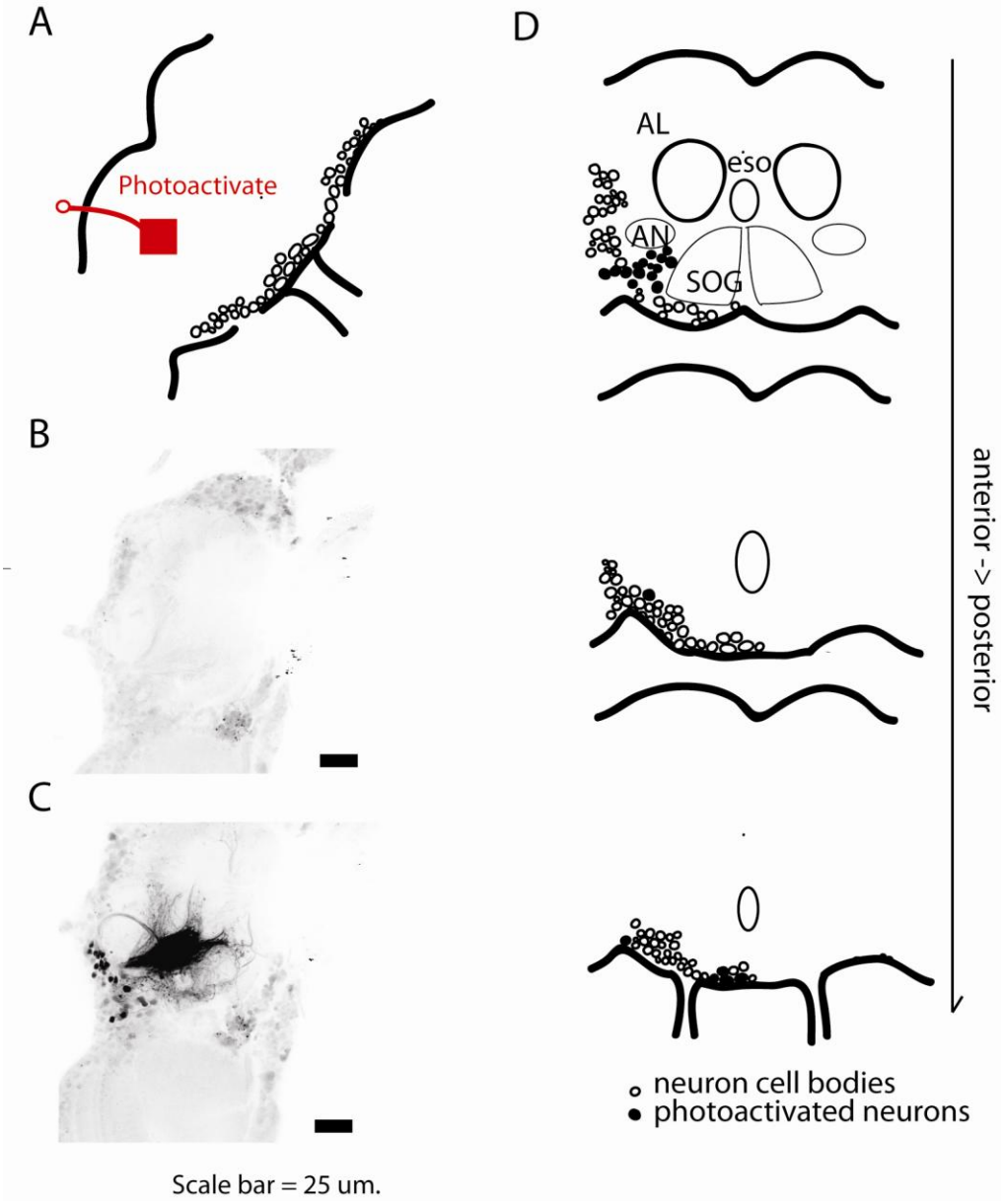

Figure 3.2: An approach to identifying second-order auditory neurons based on PA-GFP photoactivation.

(A) Schematic depiction of AMMC photoactivation.

(B) Z-projection of a brain expressing PA-GFP in cholinergic neurons prior to photoactivation.

(C) Z-projection of the same volume shown in B, after photoactivation of the AMMC.

(D) Graphical depiction of the location of cell bodies identified using this method across seven experiments.

Visuals screens of GAL4 collections

Large collections of transgenic flies containing an insertion of the yeast transcription factor GAL4 ("GAL4 lines") have been created, allowing visualization and genetic manipulation of specific populations of neurons (Fischer et al., 1988). I visually screened patterns of GAL4 expression from the stocks of Julie Simpson (Janelia Farm) and Ulrike Heberlein (UCSF). I used the following criteria, which were designed to select for potential 2nd order and 3rd order auditory neurons:

1) The GAL4 expression pattern must show signal in the Antennal Motor and Mechanosensory Center (AMMC) or the ventrolateral Protocerebrum, an area we identified as a potential input site for 3rd order auditory neurons.

2) Processes in the AMMC must be tracable to the cell body of a central neuron. This criterion eliminated very broadly expressing lines and lines that labeled the primary auditory neurons.

Screening of approximately ~1700 lines led to the identification of GAL4 drivers that labeled four classes of candidate central auditory neurons: the Giant Fiber Neuron (GFN), the Giant Commissural Interneuron (GCI), the B1 neuron, and the VLPR1 neuron. In addition, we were given a GAL4 line that labeled the GFN by our collaborator Aynn-Shyn Chiang. The results of all these efforts are summarized in Table 3.1. The next section describes electrophysiological characterization of the GFN, GCI, and B1 neurons.

Table 3.1: Lines labeling candidate auditory neurons

Line	Chromosome	Labeled Neurons
183-GAL4	II	AMMC-B1, VLPR1
a171-GAL4	?	AMMC-B1
G0117-GAL4		GFN, GCI
G0066-GAL4		GFN
CG8916-GAL4	II	AMMC-B1
4-64-GAL4		VLPR1
9-58-GAL4		GCI

Intrinsic properties and connectivity of the B1 neuron

Two GAL4 lines identified in our screen labeled the B1 neuron, which extends processes in the ipsilateral Antennal Motor and Mechanosensory Center in the region where the Group B JONs terminate. Behavioral responses to courtship song in males are abolished by silencing Group B JONs, suggesting that the B1 neuron may be involved in the perception of courtship song. We were unable to test the behavioral consequences of loss of B1 neuron function in this paradigm, as ricin-mediated cell death, RNAi-mediated knockdown of voltage-gated sodium

channels, or expression of a consitutively active version of the potassium channel Kv2.1 all resulted in death prior to eclosion (data not shown).

The cell bodies of the B1 neurons are located on the anterior surface of the brain, directly posterior to antennae themselves. Due to their close physical proximity, we were unable to make patch clamp recordings from the B1 neurons in a preparation where the antenna was free to rotate. Instead, I made whole-cell current-clamp recordings in a reduced *ex vivo* preparation from B1 neurons, targeting the patch pipette to those expressing GFP under the control of CG8916-GAL4 (Figure 3.2A). Simultaneous electrical stimulation of the antennal nerve with second pipette elicited an EPSP that arrived with a delay of 3-4 ms and was sensitive to tetrodotoxin (Figure 3.2B). A synaptic response was observed in 6/6 recordings, indicating that the B1 neuron receives input from axons in the antennal nerve, consistent with a monosynaptic connection between Group B JONs and the B1 Neuron (Figure 3.2C).

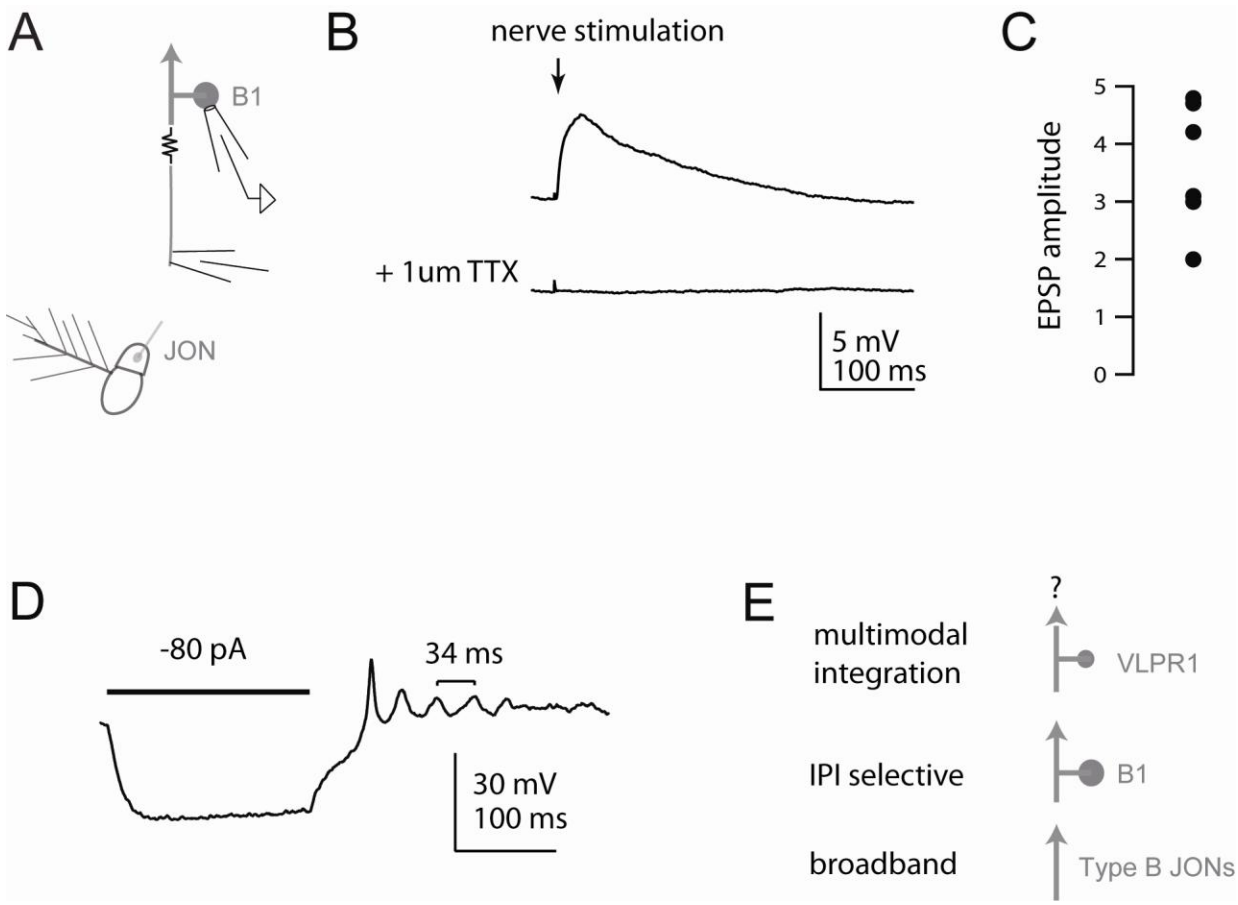

Figure 3.3: Connectivity and physiology of the B1 Neuron.

(A) A schematic showing the experimental configuration in (B). The antennal nerve was stimulated with a stimulation electrode while and *in vivo* whole-cell patch clamp recording was made from the B1 soma.

(B) Stimulation of the antennal nerve produces an EPSP in the B1 neuron.

(C) Group data (n=5) showing the amplitude of the EPSP evoked in the B1 neurons across all experiments.

(D) Representative trace showing intrinsic oscillations in the B1 neuron upon relief from a hyperpolarizing current injection. These oscillations were observed in two of five recordings.

(E) A schematic of the proposed function of several neurons in the Group B JON pathway.

Hair cells in the turtle cochlea achieve their frequency selectivity in large part through an intrinsic electrical resonance (Art et al., 1986; Crawford and Fettiplace, 1981). The resonance is generated by the dynamics of potassium and calcium conductances, and the resonant frequency of each hair cell seems to be determined by the time course of the potassium conductance (Art et al., 1986). Negative current injection into the hair cell produces a hyperpolarization, followed by a damped fluctuation of the membrane potential at the intrinsic resonance frequency. Remarkably, this phenomenon is observed in the B1 neurons as well (Figure 3.2D). In a minority of recordings, the resonance frequency of the oscillation was identical to that of the reported inter-pulse-interval of the Drosophila courtship song (Schilcher, 1976). Thus, B1 neuron electrical resonance is a possible mechanism that may produce selectivity to the conspecific song. In this model, the function of the B1 neurons is to act as a bandpass filter centered on the inter-pulse interval of the conspecific song. Activation of the B1 neuron triggers activity in the VLPR1 neuron, which innervates an area of neuropil that also receives input from gustatory sensory neurons that function during courtship (Miyamoto and Amrein, 2008). It is tempting to speculate that the multimodal sensory cues that impinge on the fly are integrated in the ventrolateral protocerebrum (Figure 3.2E).

The Giant Commisural Interneurons and Giant Fiber Neurons are central auditory neurons

The Giant Fiber Neuron (GFNs) and Giant Commisural Interneurons (GCIs) are identified neurons that are thought to form part of a visual escape circuit (Koto et al., 1981).

Each GFN is coupled through to 2-3 GCIs, which in turn project to the contralateral GFN (Phelan et al., 2008). Together, these neurons receive visual and mechanosensory input and make electrical synapses with neurons in the thoracic ganglion that control the action of jump and flight muscles (Phelan et al., 1996). *In vivo* optogenetic stimulation of the Giant Fiber System results is sufficient to elicit escape-like behavior, but the Giant Fiber System is not required for visually-evoked escape (Card and Dickinson, 2008; Lima and Miesenbock, 2005).

As mentioned previously, anatomical evidence suggested that the GFN might also function as a central auditory neuron. To test this possibility, we made *in vivo* whole-cell patch-clamp recordings from the GFN under conditions where we could also provide an acoustic stimulus (Figure 3.4A). In the absence of sound stimuli, we observed hundreds of spontaneous excitatory events in the GFN every second (Figure 3.4B). Pure tone stimuli caused excitatory currents to arrive in oscillatory bursts. When we fixed the third antennal segment with a drop of glue, spontaneous events persisted but the response to sound was abolished (Figure 3.4B). Removing the antennae eliminated both spontaneous events and sound responses (Figure 3.4B).

The geometry of the antennal receiver suggested that it might be intrinsically direction selective: particle velocity stimuli that are oriented orthogonally to the plane of the arista might produce more movement than those oriented in other directions. To test whether the GFN receives input from directionally-selective JONs, I recorded responses to courtship song from the GFN under conditions when only one antenna was intact. Consistent with this idea, sounds from the contralateral sound field were more effective at driving GFN activity than those from the ipsilateral sound field (Figure 3.4D) Measurements of the trial-average current produced in responses to various speaker locations (-120 degrees to 120 with respect to midline) showed a loss of sensitivity as the angle between the aristal plane and speaker grew more oblique (Figure

3.3D). This data shows that the GFN receives input from direction-selective JONs and indicates that this may be a consequence of the aristal geometry. Sound localization is a challenge for organisms with small inter-aural distances (Robert et al., 1996). Our data suggests that the fly may infer the location of a sound source from the particle velocity vector, thereby overcoming this limitation.

Figure 3.4: The Giant Fiber Neuron is a central auditory neuron.

(A) Schematic showing a Johnston's organ neuron (JON) antenna whose axon projects into the brain and is connected via gap junctions with the dendrite of the Giant Fiber Neuron (GFN). The GFN sends an axon into the thorax (arrow). In vivo whole-cell patch clamp recordings were made from the GFN soma.

(B) Spontaneous and evoked currents recorded in the GFN during presentation of a sound stimulus (100 Hz, 0.0024 m/sec). Stabilizing the antennae by glueing the second and third antennal segments together abolishes sound responses but not spontaneous events. Removing the antennae abolishes both spontaneous events and sound responses.

(C) Trial-averaged responses to three bouts of courtship song recorded in the GFN with only one antenna intact (see schematic). The speaker was placed on a rotary stage mounted in the condenser holder, permitting changes to in the location of the acoustic stimulus. Reponses to the contralateral sound field are stronger than the ipsilateral sound field, demonstrating that the antennal receiver is intrinsically direction-selective.

(D) Group data (n=6) showing the direction selectivity of the antenna for the three sound levels in (C).

Figure 3.4 (continued): The Giant Fiber Neuron is a central auditory neuron.

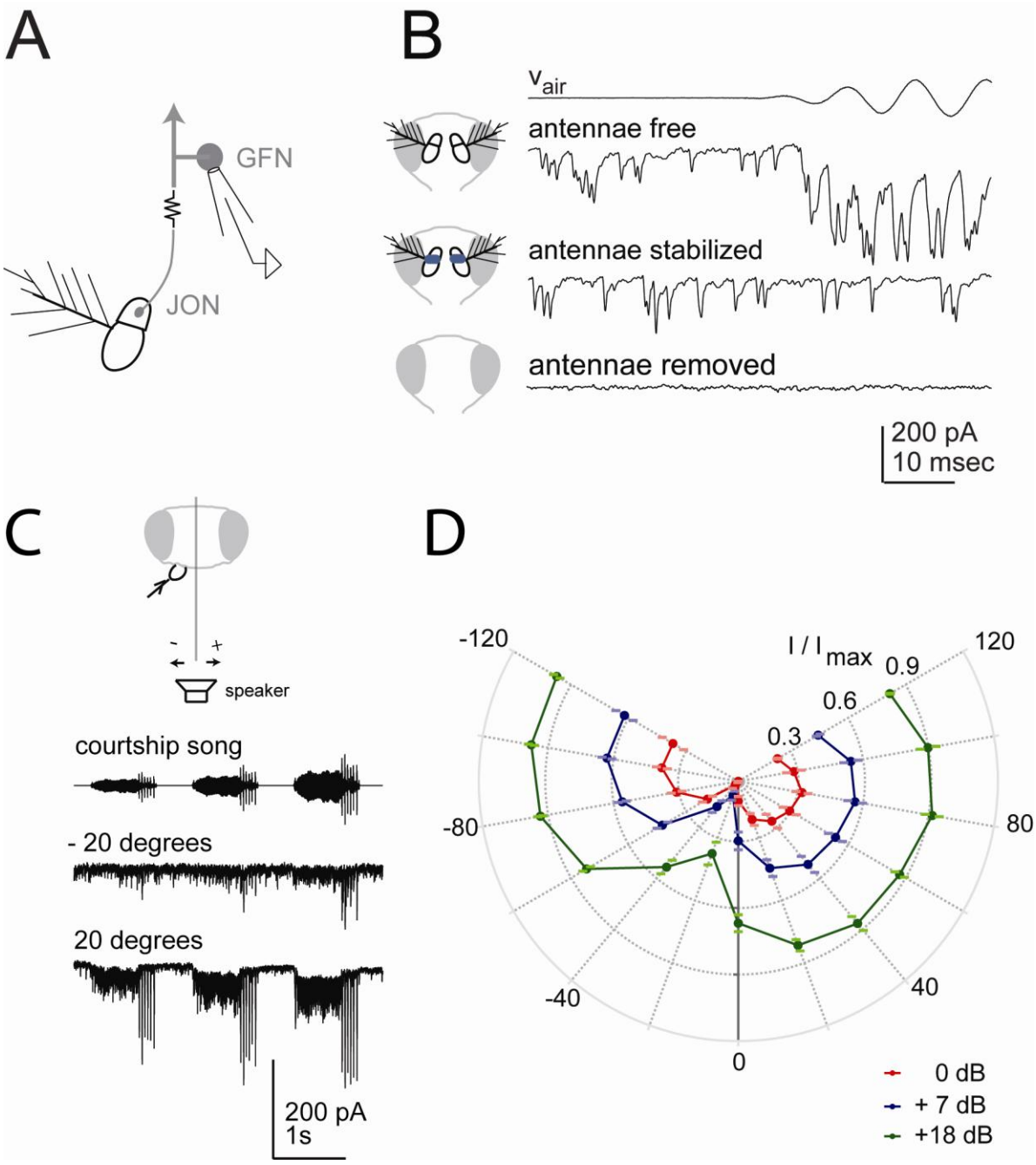

3.3 Discussion

We identified three neurons of interest: the B1 neuron, its likely postsynaptic particle VLPR1, and the GFN (Table 3.1). *In vivo* whole-cell recordings were only possible in the GFN, which was excited by sound and showed frequency doubled responses, but no apparent selectivity to courtship song. Currents recorded in the GFN were directionally sensitive when the contralateral antenna was removed. Responses were larger for particle velocity stimuli that were oriented orthogonally to the aristal plane. Currents recorded with both antennae intact were only weakly directionally selective, indicating that the GFN is able to sum activity over both antennae.

Recordings from the Giant Fiber Neuron formed the basis of the work in Chapter 4 and Chapter 5, which examine the mechanism of auditory transduction in *Drosophila*.

Chapter 4

A sensitive measure of Drosophila auditory transduction

ATTRIBUTIONS: This chapter is a modified version of a manuscript that has been submitted for publication as "Lehnert BP, Baker AE , Gaudry Q, Chiang A-S, and Wilson RI. Distinct roles of TRP channels in auditory transduction and amplification in *Drosophila.*"

A.E.B. performed and analyzed the behavioral experiments in Figure 4.1, panels A-D with technical assistance from Q.G. and myself. I collected and analyzed the remainder of the data in this chapter.

4.1 Introduction

Attempts to record directly from individual JONs in a hearing preparation have been unsuccessful due to the fact that these are small cells embedded in a delicate structure whose integrity is critical to their function. We therefore developed a novel method for recording signals non-invasively from JONs, with the ultimate goal of recording the signals that give rise to action potentials. We reasoned that we might be able to achieve this by recording from the Giant Fiber Neuron (GFN), a single identifiable central neuron that extends dendrites into the region of the brain where JON axons terminate (Kamikouchi et al., 2009). A recent study has shown that the GFN responds to auditory stimuli (Tootoonian et al., 2012). What distinguishes the GFN from other central auditory neurons is the finding that dye loaded into JONs can diffuse directly into the GFN, implying that it is coupled to the JON by gap junctions (Strausfeld and Bassemir, 1983). Consistent with this, there is ultrastructural evidence that JONs form gap junctions with some central neurons (Sivan-Loukianova and Eberl, 2005). Thus, we made *in vivo* whole-cell patch clamp recordings from the GFN to ask whether it receives direct electrical input from JONs via gap junctions. We made these recordings in voltage-clamp configuration to minimize cable filtering by the GFN dendrite, and to minimize the contribution of active conductances in the GFN.

Prior electrophysiological, mechanical, and behavioral measures have led to different impressions of the sensitivity of the *Drosophila* auditory system (Card and Dickinson, 2008; Gopfert et al., 2006; Lima and Miesenbock, 2005; Schilcher, 1976). Determining the sensitivity of the *Drosophila* auditory system is necessary for understanding the neural basis of acoustic communication and has important implications for the mechanism of transduction. Therefore, we characterized the mechanical, electrophysiological, and behavioral sensitivity of the fly auditory system. We began by asking what sound intensities elicit a behavioral response. Behavioral measurements are important because they set an upper bound on the neural threshold.

4.2 Results

Drosophila hearing is sensitive to low-intensity sounds

Virtually all studies to date have measured behavioral thresholds in the context of courtship, under conditions where it is difficult to precisely control the intensity of stimulation. We reasoned that a simple acoustic startle reflex might yield lower estimates of the threshold. We tethered flies and suspended them above a small plastic ball floating on a cushion of air (Figure 4.1A). The fly's fictive velocity was measured by optically monitoring the movement of the ball. Calibrated sound stimuli (Figure 2.1) were delivered from a speaker in front of the fly. In this apparatus, the flies tended to run spontaneously, alternating with brief bouts of standing still. In response to tone pips, the fly tended to transiently slow or stop their forward running (Figure 4.1B).

Figure 4.1: Drosophila hearing is sensitive to low-intensity sounds.

(A) Measurement of the acoustic startle response. A tethered fly faces a speaker while standing on a spherical treadmill.

(B) The fly's fictive forward velocity plotted versus time. The gray box represents the time of the sound stimulus (300 Hz tone, played at an intensity of 0.0055 m/sec). Shown are three individual trials (in one of which the fly was not moving), plus an average of 27 trials for this condition.

(C) Responses to sound grow with sound intensity. Arrowhead indicates the lowest intensity where the forward velocity during the tone was significantly different from the forward velocity immediately prior to the tone ($p<0.05$, paired t-test with iterative Bonferroni correction, n=19–27 flies).

(D) Fixing the antenna in place with adhesive reduces the behavioral response to sound ($p<0.0005$, t-test, n=19 free and n=7 fixed). Within each fly, the responses to all stimulus intensities were averaged together prior to statistical testing, and SEM was computed across flies on this averaged data.

(E) Selective RNAi-mediated knockdown of voltage-gated sodium channels in JONs reduces the response to sound ($p<0.01$, t-test, n=11 control and 11 knockdown). As in panel D, responses were averaged across all stimulus intensities.

(F) Field potential recordings from the antennal nerve in response to ramped 300 Hz tones of increasing particle velocity (corresponding to every other intensity in panel G). The acoustic particle velocity waveform recorded in the vicinity of the fly (vair) is shown at top.

(G) The field potential response (quantified as the signal at twice the sound frequency, normalized to the maximum in each experiment) is plotted as a function of sound intensity (black circles). The open black circle shows the background noise at 300 Hz in the vicinity of the preparation and the corresponding field potential. Arrowhead indicates the response to the least intense sound that was significantly different from the response to background ($p<0.05$, Wilcoxon rank sum tests with sequential Bonferroni correction). The sensitivity of antennal movement is also shown as a function of sound intensity (magenta). Sensitivity is computed as the ratio of antennal angular velocity (in radians/sec) to acoustic particle velocity amplitude (in m/sec).

Figure 4.1 (continued): Drosophila hearing is sensitive to low-intensity sounds.

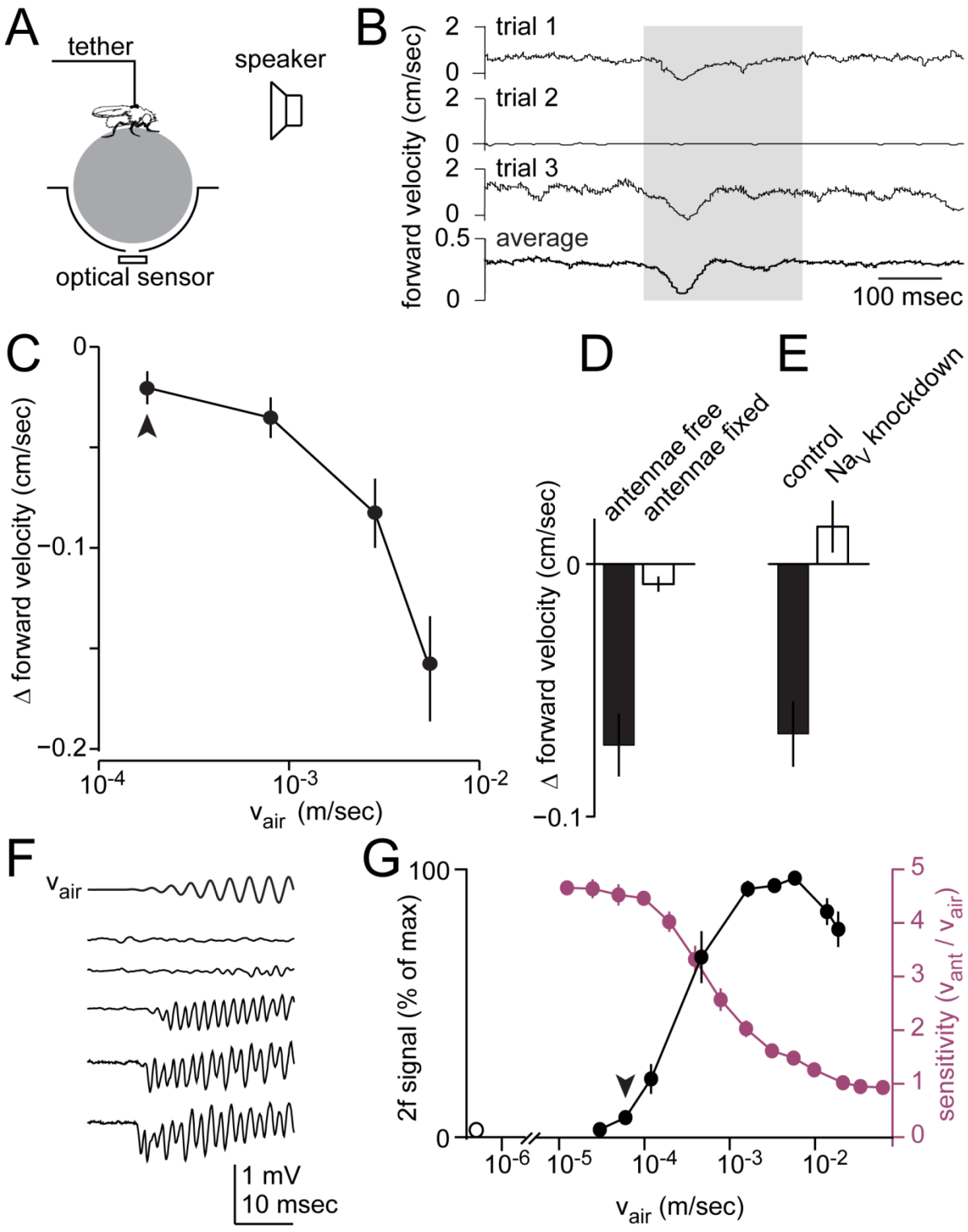

We observed startle behavior in response to sounds as soft as 1.2×10^{-4} m/sec, or 65 dB SVL (Figure 4.1C). This threshold is lower than that estimated previously using courtship behaviors (Card and Dickinson, 2008; Lima and Miesenbock, 2005; Schilcher, 1976), and is similar to that recently reported using a conditioned proboscis response reflex (Menda et al., 2011). This result means that the most sensitive JONs must have thresholds at or below this intensity. It also demonstrates that these intensities are behaviorally relevant.

We verified that startle behavior was abolished when we stabilized the most distal antennal segment with a drop of glue (Figure 4.1D). It was also attenuated when we suppressed spiking in JONs by selective RNAi-mediated knockdown of voltage-dependent sodium channels (Sukharev et al., 1994) under the control of a JON-specific Gal4 line (Figure 4.1E; see also Figure 4.2). Thus, the startle behavior requires sound-evoked spiking in JONs.

As an initial measurement of neural thresholds, we made field potential recordings from the antennal nerve. Sounds elicited field potential oscillations at twice the stimulus frequency (Figure 4.1F), as previously reported (Eberl et al., 2000a). For the 300 Hz tone, 5.7×10^{-5} m/sec (58 dB SVL) was the softest intensity that elicited a response significantly above the response to background noise (Figure 1G, $p<0.05$, *t*-test, $n=6$). As expected, the neural threshold is lower than the behavioral threshold.

We also used laser Doppler vibrometry to measure antennal movements in response to these sounds. In agreement with previous studies (Gopfert et al., 2006; Gopfert and Robert, 2003), we observed a nonlinearity in the antenna's movement as sound intensity increased. Specifically, antennal movements (normalized to air particle velocity movements) were largest

for weak sounds, and became smaller for loud sounds (Figure 4.1G). This phenomenon implies active amplification of movements produced by weak sounds. It is notable that active amplification is observable in a range of intensities too weak to produce antennal field potential responses (Figure 4.1G). This suggests that active amplification may be a process distinct from transduction, rather than being a hallmark of transduction, and motivates the need for a sensitive measure of JON activity.

Spikes from auditory receptor neurons propagate into the Giant Fiber Neuron through gap junctions

In the absence of sound stimuli, we observed hundreds of spontaneous excitatory events in the GFN (Figure 4.22B) every second. Events that were well-isolated in time had a stereotyped profile within a fly and across flies, and were very fast (<1 msec half-width, Figure 2C). Pure tone stimuli caused excitatory currents to arrive in oscillatory bursts at twice the sound frequency, similar to the frequency doubling observed in the antennal nerve field potential (Figure 4.1H, 4.1B). When we fixed the third antennal segment with a drop of glue, spontaneous events persisted but the response to sound was abolished (Figures 4.2B). Removing the antennae eliminated both spontaneous events and sound responses (Figures 4.2B). These results imply that spontaneous events arise in antennal neurons and – because they are modulated by sound – likely originate in JONs. The speed and stereotypy of these events suggest that they represent action potentials in JONs (where the membrane potential is unclamped) which then propagate into the GFN via gap junctions.

We used pharmacological and genetic manipulations to further investigate how these events propagate into the GFN. Blocking chemical synaptic transmission (with bath application

Figure 4.2: Spikes from auditory receptor neurons propagate into the Giant Fiber Neuron through gap junctions.

(A) Schematic showing a Johnston's organ neuron (JON) antenna whose axon projects into the brain and is connected via gap junctions with the dendrite of the Giant Fiber Neuron (GFN). The GFN sends an axon into the thorax (arrow). In vivo whole-cell patch clamp recordings were made from the GFN soma.

(B) Spontaneous and evoked currents recorded in the GFN during presentation of a sound stimulus (100 Hz, 0.0024 m/sec). Stabilizing the antennae by glueing the second and third antennal segments together abolishes sound responses but not spontaneous events. Removing the antennae abolishes both spontaneous events and sound responses.

(C) Well-isolated spontaneous events show a stereotyped shape and size (top, same cell as in B). The average shape of these events is also stereotyped across cells (bottom, 9 average events scaled to the same peak).

(D) Representative recordings show that, relative to baseline, event rates are unaffected by pharmacological blockade of chemical synapses (200 μM Cd2+) but abolished by blocking spiking (2 mM TTX) and greatly reduced by selective transgenic knockdown of voltage-gated sodium channels in JONs. Recorded events are also abolished by a mutation in the gap junction subunit shakB.

(E) Group data showing the rate of spontaneous events for each manipulation. Each circle is a different experiment, and lines connect measurements from the same experiment. All manipulations produce a significant reduction ($p<0.05$, paired or unpaired Wilcoxon rank sum tests with Bonferroni correction), except for Cd2+.

(F) A click stimulus elicits a microphonic potential in the vicinity of the fly (top), followed rapidly by a field potential deflection in the antennal nerve (blue) and an inward current in the GFN (magenta). Neural responses are averages of many trials. Latencies from click arrival (calculated as the time when the response reached 10% of maximal) are shown for all antennal nerve (n=7) and GFN recordings (n=6) at bottom. The delay between the average field potential latency and average GFN latency is 271 μsec. This value includes the time required for the electrical signal to propagate from the antenna (where the field potential is recorded) down the antennal nerve and into the brain.

Figure 4.2 (continued): Spikes from auditory receptor neurons propagate into the Giant Fiber Neuron through gap junctions.

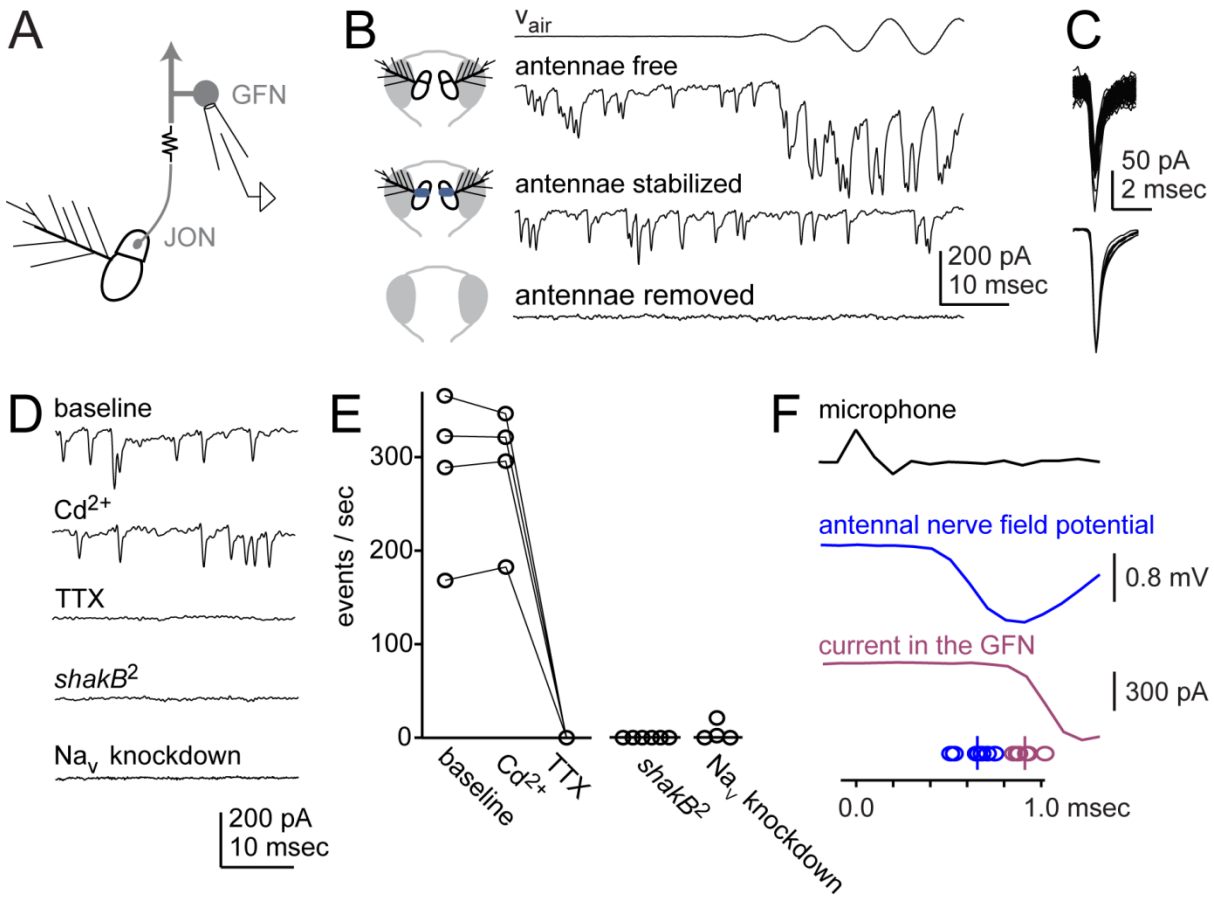

of Cd^{2+}) had no effect (Figure 4.2D,E). We note that this manipulation blocks chemical synaptic transmission in the *Drosophila* olfactory system (Kazama and Wilson, 2008). By contrast, blocking spikes (with bath application of tetrodotoxin) eliminated spontaneous events, as did RNAi-mediated knockdown of voltage-gated sodium channels selectively in JONs (Figures 4.2D,E, 4.3). Together, these results demonstrate that sodum channel knockdown in the GFN alone has no effect on the sound-evoked currents recorded in the GFN in voltage-clamp mode. Moreover, events were virtually eliminated by a mutation in the gap junction subunit ShakB (Figure 4.2D,E), a mutation which disrupts electrical synapses in the visual and olfactory systems (Curtin et al., 2002; Phelan et al., 1996). Finally, the latency from JON spiking to the appearance of currents in the GFN is <300 microseconds (Figure 4.2F). Together, these findings are strong evidence that events are individual JON spikes, rather than synaptic events, and that they propagate into the GFN via electrical synapses.

Figure 4.3: Knocking down DmNav in the GFN alone does not change recorded GFN currents.

In experiments where we knocked down sodium channel expression in JONs, we also needed to use Gal4-UAS to label the neurons of the Giant Fiber System with GFP. For this reason, the knockdown transgene was expressed in the Giant Fiber System as well as in JONs. To assess whether the observed phenotype was due to DmNav knockdown in the Giant Fiber System or in JONs, we performed control experiments where the JON-specific Gal4 driver was omitted, and thus the knockdown transgene was expressed in the Giant Fiber System but not JONs.

(A) Representative single trials showing a spike-mediated sound response in a wild type recording (stimulus is a 300 Hz tone, intensity 0.0024 m/sec, timing indicated by horizontal line, no TTX in the bath). Genotype is G0117-GAL4,UAS-CD8:GFP.

(B) Same as above, but for a fly where sodium channel expression is knocked down in the GFN but not JONs. Genotype G0117-GAL4,UAS-CD8:GFP/UAS-dicer2;+;UAS-DmNav-RNAi /+.

(C) Same as above, but for a fly where sodium channel expression is knocked down in JONs as well as the GFN. Genotype is G0117-GAL4,UAS-CD8:GFP/UAS-dicer2;nan-GAL4/+;UAS-DmNav-RNAi /+. Two examples are shown from different flies, illustrating the variable penetrance of the knockdown phenotype.

(D) Group data showing the average spike-evoked current. Each point represents a different fly, with responses averaged across equal numbers of trials for each of three frequencies (100 Hz, 200 Hz, 300 Hz, all 0.0024 m/sec, total of 9 - 35 trials per fly). There was a significant difference in the mean of the evoked current across groups (1-way ANOVA, $p<0.001$). There was a significant difference between the genotype with JON knockdown and the other two groups ($p<0.005$), but not between wild type and knockdown in the Giant Fiber System alone ($p=0.27$) Statistical tests are multiple pairwise t-tests with Holm adjustment.

Figure 4.3 (continued): Knocking down DmNav in the GFN alone does not change recorded GFN currents.

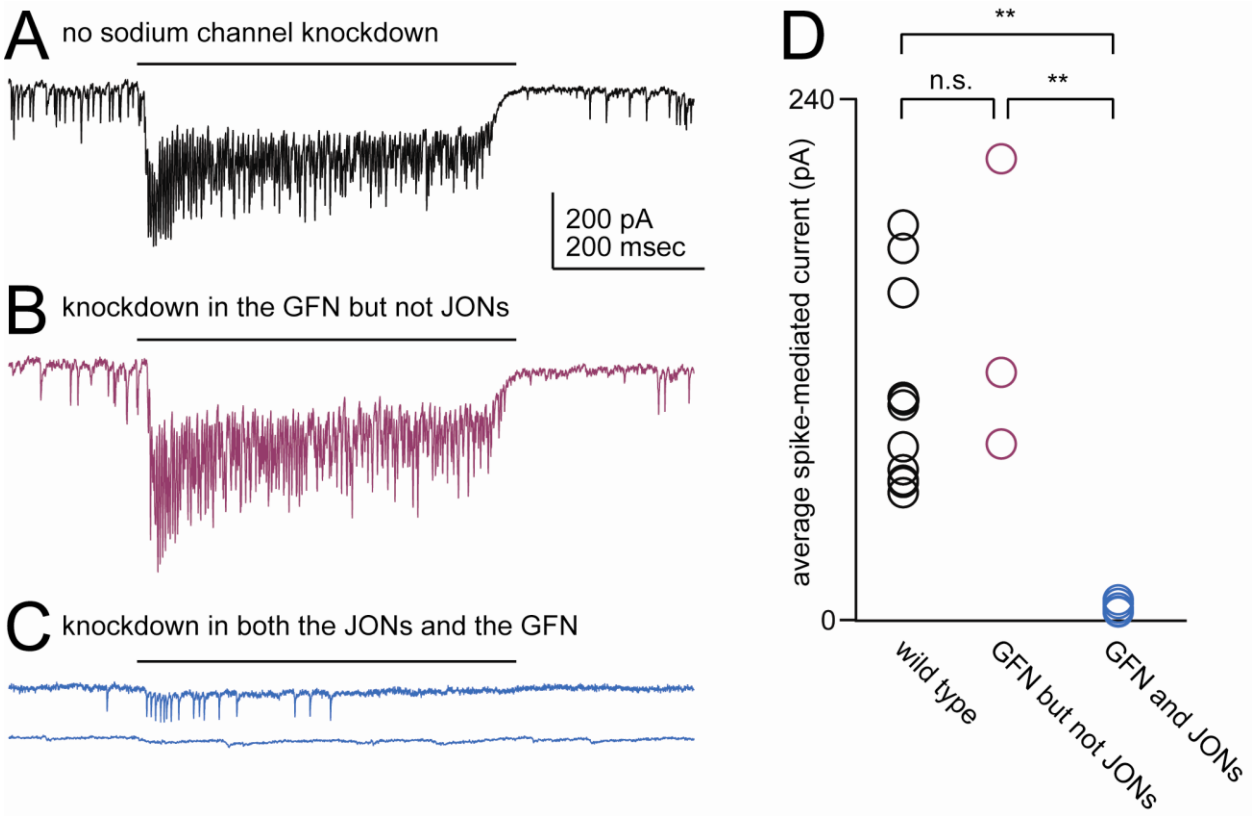

Subthreshold signals from auditory receptor neurons propagate into the Giant Fiber Neuron

Next we asked whether we could use GFN recordings as a way to monitor the sound-evoked subthreshold signals in JONs that give rise to spikes. To block spikes, we bath-applied TTX, which reduced sound-evoked currents to about 5% of their original level (Figure 4.4A). In experiments where we selectively knocked down voltage-gated sodium channels in JONs, we observed sound-evoked currents similar to those recorded in wild type flies with TTX in the bath (Figure 4.4B, C). This argues that the effect of TTX on the sound-evoked currents is due to the blockade of spiking JONs, rather than blockade of spiking in other, unidentified neurons. The currents recorded in TTX thus reflect the subthreshold activity in JONs that normally gives rise to JON spikes. We will term these "generator currents".

Both spike-mediated currents and generator currents are sensitive to weak sound intensities (Figure 4.4D, E). Notably, whereas the spike-mediated currents decline at high intensities, the generator currents show a smooth monotonic dependence on sound intensity. This indicates that the decline in the spike-mediated currents is due to spike frequency adaptation, and not adaptation in transduction. Also, whereas spike-mediated currents are selective for the pitch of the sound stimulus (with higher pitches producing smaller responses), the generator currents are less so. This implies that some of the frequency selectivity in spike-mediated currents is due to an inability to generate spikes efficiently at high pitches, again probably due to spike adaptation.

Figure 4.4: Subthreshold signals from auditory receptor neurons propagate into the Giant Fiber Neuron.

(A) Sound-evoked currents from a representative experiment. All traces are averages of many trials, and thus spontaneous activity is averaged out, leaving only the sound-locked response. Blocking chemical synapses (200 mM Cd2+) had no effect, but blocking spikes (2 mM TTX) reduced sound-evoked currents by ~95%.

(B) Sound-evoked generator currents. The recording in TTX (top) is the same as in A, but displayed on an expanded vertical scale. In a recording where voltage-gated sodium channels were selectively knocked down in JONs (bottom), the result is similar to bath application of TTX.

(C) Group data showing the magnitude of currents recorded in response to a 100Hz tone (0.00244 m/sec) for each manipulation. Each circle is a different experiment, and lines connect measurements from the same experiment.

(D) Mean sound-evoked currents (recorded in the absence of TTX) as a function of sound intensity (n=8).

(E) Mean sound-evoked generator currents (recorded in TTX) as a function of sound intensity (n=8). Note that TTX eliminates the decrease in responses at high sound intensity, indicating that this decrease is likely due to spike adaptation in JONs.

(F) Mean sound-evoked generator currents (recorded in TTX) plotted against sound-evoked

antennal rotation (same experiments as in E). Note that frequency tuning is essentially

eliminated.

Figure 4.4 (continued): Subthreshold signals from auditory receptor neurons propagate into the Giant Fiber Neuron.

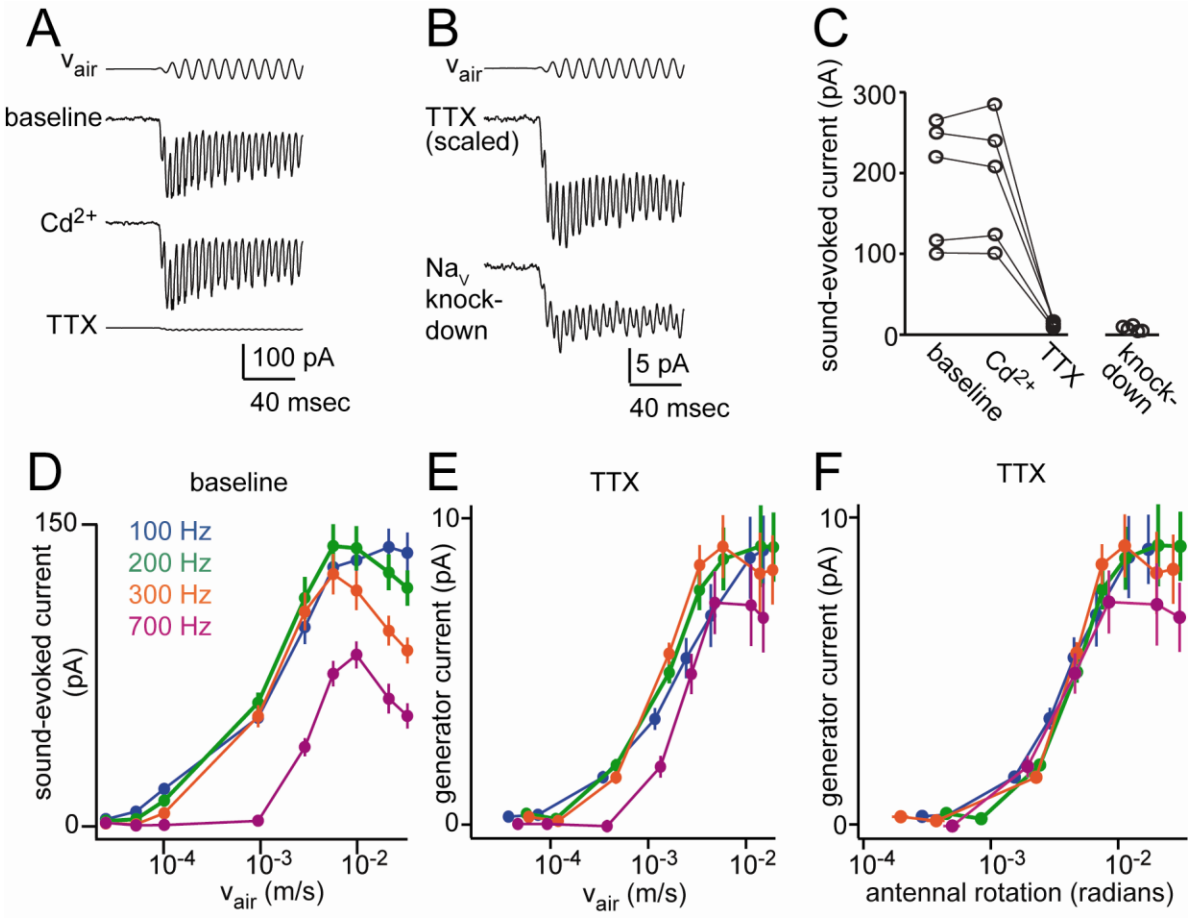

To understand how transduction depends on antennal rotation, we measured rotations in response to these sound stimuli using laser Doppler vibrometry of the antennae. Interestingly, plotting generator currents as a function of antennal rotation (Figure 4.4F) reveals a monotonic relationship which is essentially frequency-independent. This indicates that the apparent frequency selectivity of the generator currents is due to the frequency selectivity of the antenna, which has a resonant frequency around 160 - 300 Hz at low sound intensities (Gopfert and Robert, 2002b, 2003). When this effect is removed by reducing the data to a current-rotation curve, it becomes clear that there is a single underlying relationship between transduction and antennal movement. In the remainder of this study, we will focus on how TRP channels specify this relationship.

Spikes and generator currents arise from an identified genetic population of receptor neurons

JONs were initially subdivided into types based on the observation that different JONs project to different brain regions (Kamikouchi et al., 2006). Calcium imaging studies have subsequently shown that type AB JONs have a relatively low threshold for sound stimuli, whereas type CE JONs have a relatively high threshold for sound stimuli (Effertz et al., 2011; Kamikouchi et al., 2009). A calcium imaging study has also reported that NompC is absolutely required for sound responses in type AB JONs, whereas NompC is dispensable for sound responses in CE JONs (Effertz et al., 2011). However, all JONs express NompC, Nanchung, and Inactive (Gong et al., 2004; Lee et al., 2010), leading to speculation that these TRPs might play different roles in different JON types (Effertz et al., 2011).

Given these considerations, we sought to clarify which JON types give rise to the signal that we are recording. We filled the GFN with a biocytin marker in flies where type AB JON axons were labeled with GFP. We observed multiple areas of overlap between the GFN dendrite and the labeled JON axons (Figure 4.5A). By contrast, type CE JON axons did not contact the GFN dendrite (Figure 4.5A). This result confirms an earlier study showing that the GFN dendrites arborize in the region where type AB axons terminate (Kamikouchi et al., 2009). These findings predict that the GFN receives input from AB but not CE axons.

We next tested whether the GFN is functionally connected solely to type AB JONs, or whether type CE JONs also provide input to the GFN. This could be the case if an indirect connection existed between type CE JONs and the GFN. We created flies where just one of the two types of JONs is functional, by virtue of cell-specific rescue of *inactive* in an *inactive* mutant background. As a positive control, we confirmed that rescuing *inactive* expression in most or all JONs was able to rescue the mutant phenotype in GFN recordings (Figure 4.5B,C). When we rescued *inactive* selectively in type AB JONs, we also observed complete rescue, and these recordings were indistinguishable from wild type or pan-JON rescue (Figure 4.5B, C). By contrast, rescuing *inactive* selectively in type CE JONs had no effect, equivalent to flies where the Gal4 driver was omitted (Figure 4.5B, C). These results demonstrate that the signals we record in the GFN arise exclusively in type AB JONs.

Figure 4.5: Spikes and generator currents arise from an identified genetic population of receptor neurons.

(A) Confocal immunofluorescent images of JON axons (green) and the GFN dendrite (red). The GFN co-localizes with axons of JON-AB axons but not JON-CE axons. JONs are labeled with CD8:GFP and the GFN dendrite is filled with biocytin from the recording pipette. (In these recordings, the GFN was patched without labeling it with GFP.) An antibody against a synaptic antigen (nc82, blue) stains the synapse-rich part of the antennal mechanosensory and motor center (dotted elipse) and the antennal lobe (AL). Images are z-projections through a 3-mm depth. Inspection of the entire stack showed multiple points of contact between labeled JONs and the GFN.

(B) Representative single trials showing spontaneous events and spike-mediated sound responses in wild type and inactive mutant flies, as well as in flies where inactive is rescued in all JON types (under the control of nanchung-Gal4), in type AB JONs (under the control of JO-AB-Gal4), and in type CE JONs (under the control of JO-CE-Gal4).

(C) Group data showing that rescue of inactive in type AB JONs is sufficient to completely restore spontaneous events, spike-mediated sound responses, and generator current sound responses. There is a difference in the mean values of all three metrics across groups (1-way ANOVA, $p < 0.001$ for all three measures). The mean values of all three metrics are not significantly different between wild-type, all-JON rescue, and type AB rescue (Tukey's HSD, $p > 0.05$, n=4, 5, and 6). Similarly, the values of all three metrics are not significantly different in type CE rescue and the iav mutants (Tukey's HSD, $p > 0.05$, n=6 for rescue in CE, 4 for inactive mutants). There is a significant difference in all three metrics between the members of these two subsets.

Figure 4.5 (continued): Spikes and generator currents arise from an identified genetic population of receptor neurons.

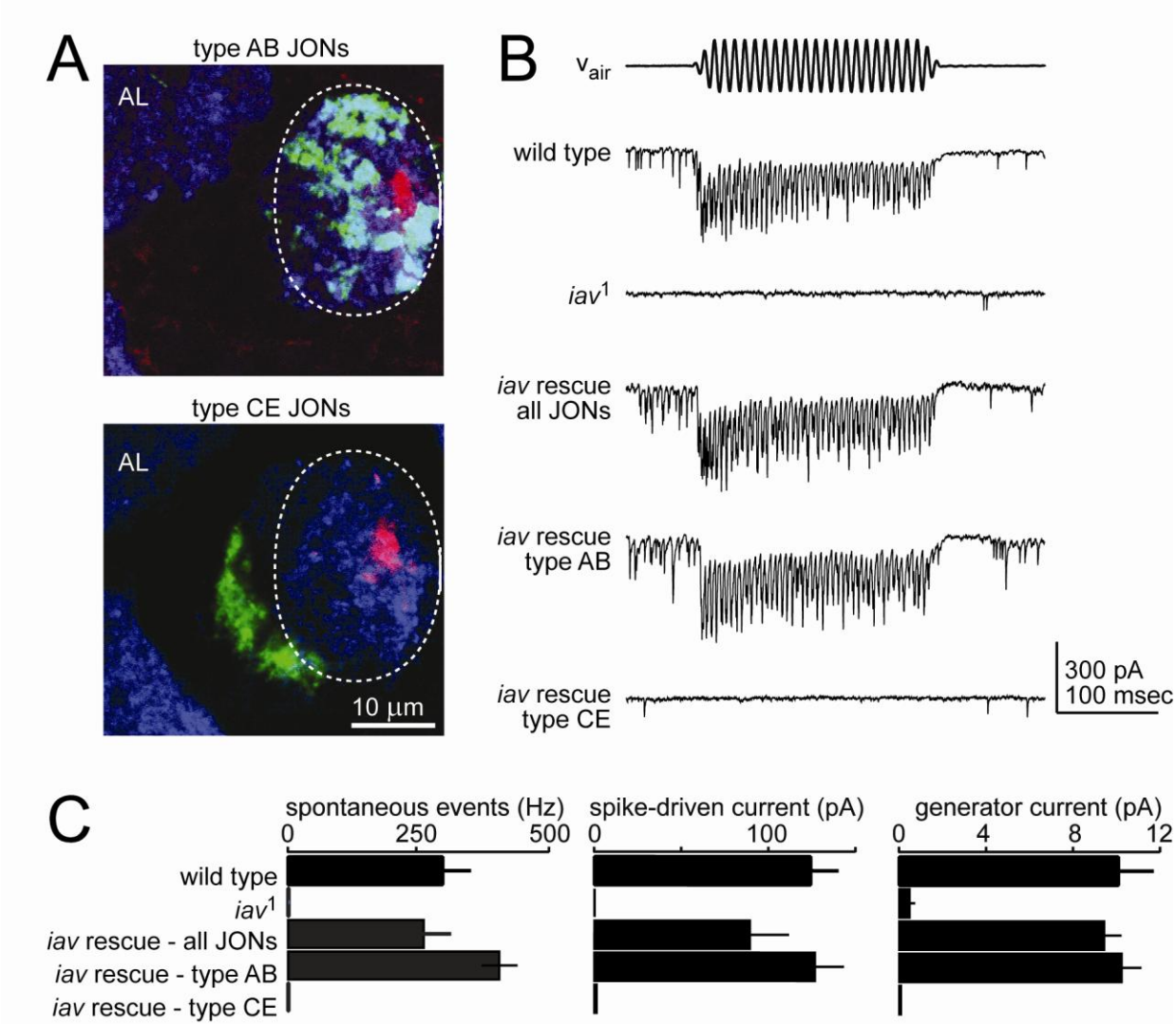

4.3 Discussion

A sensitive measure of auditory receptor neuron activity

In this study, we showed that relatively low-intensity sounds (i.e., lower-intensity than previously used to study courtship behavior) can elicit a behavioral response in *Drosophila*. This provides a motivation for investigating *Drosophila* auditory transduction near absolute threshold, and in particular the mechanisms that specify the sensitivity of the transduction complex. This in turn requires developing a sensitive method for measuring transduction currents from type AB JONs, the receptor neurons which are most sensitive to sound (Kamikouchi et al., 2009; Yorozu et al., 2009). Our anatomical and genetic data demonstrate that GFN currents are a selective measure of activity in type AB JONs.

Although this approach involves recording JON activity indirectly via the GFN, the currents we record are nevertheless relatively fast. Indeed, they have a shorter latency and faster rise time than some mechanosensitive currents which are recorded directly from the cells where these currents arise (e.g., Story et al., 2003). Thus, although the signals we record are likely smoothed by cable filtering, the degree of filtering is not necessarily larger than in the case where signals are recorded directly from mechanosensitive neurons. We could observe generator currents in the GFN in response to the smallest step stimulus we used, and this stimulus is essentially identical to the threshold stimulus for evoking calcium responses in JONs (Effertz et al., 2011). The threshold for evoking GFN currents was also essentially the same as the threshold for evoking an antennal nerve field potential response. Finally, these thresholds are just below the threshold for *Drosophila* auditory behavior. Taken together, these comparisons argue that our

approach is sensitive enough to report generator currents evoked by near-threshold auditory stimuli.

Chapter 5

The role of TRP channels in auditory transduction

ATTRIBUTIONS: This chapter is a modified version of a manuscript that has been submitted for publication as "Lehnert BP, Baker AE , Gaudry Q, Chiang A-S, and Wilson RI. Distinct roles of TRP channels in auditory transduction and amplification in *Drosophila.*"

I collected and analyzed the data in this chapter.

Introduction

It has been proposed that Nanchung and Inactive function to amplify subthreshold transduction currents to the level of spike initiation (Gopfert et al., 2006; Kamikouchi et al., 2009; Lee et al., 2010; Nadrowski et al., 2008). In this model, NompC is required for transduction and is the likely candidate for the auditory transduction channel. We tested these propositions by recording generator currents using the techniques described in Chapter 4.

Results

Loss of Nanchung or Inactive abolishes generator currents

If Nanchung and Inactive function as amplifiers of a transduction current, we should be able to measure generator currents in *nanchung* and *inactive* mutant flies. Contrary to the prediction of the prevailing model of transduction, we find that both spike-mediated sound responses and sound-evoked generator currents are completely absent in null mutants of either gene (nan^{36a} and iav^{1}) (Figure 5.1A, B). The rate of spontaneous events is drastically reduced in both mutants, but events are still present, and their size and shape are normal (Figure 5.1A). This result suggests that these TRPV channels are required for a resting conductance that drives spontaneous JON spiking, but it also demonstrates that neither TRPV is required for JON spikes *per se*.

Figure 5.1: Loss of Nanchung or Inactive completely abolishes generator currents.

(A) Single trials showing currents recorded in the GFN in response to a 100 Hz tone (0.0044 m/sec). In the nanchung and inactive mutants, sound responses are absent. Spontaneous events are greatly reduced in frequency as compared to wild type, but when they occur, their size and shape is similar to wild type. Insets (bottom) show the average shape and size of the isolated events in these recordings.

(B) Representative generator current recordings in the presence of TTX. Traces are averages of many trials. Generator currents are absent in the nanchung and inactive mutants. The sound stimulus is the same as in A.

(C) Frequency domain representation of the generator currents in B. The wild-type currents show a large peak at twice the sound frequency (2f) and a smaller peak at the frequency of sound stimulation (1f). The currents in both mutants show no measurable peak at 1f or 2f.

(D) Group data showing the signal at twice the sound frequency (2f) as a fold change over that present in a baseline period of equivalent length (n=18 wild type, 5 nanchung mutants, 5 inactive mutants). Each circle is one experiment, and horizontal lines are means.

(E) Confocal immunofluorescent images of JONs within the second antennal segment. An antibody that localizes to the ciliary dilation (21A6, magenta) marks the boundary between the distal and proximal dendrite of each JON. A NompC:GFP fusion protein (green) localizes properly to the distal portion of the dendrite in both genotypes, showing loss of Nanchung does not disrupt NompC localization. Images are z-projections through an 8 μm-depth, scale bar is 10 μm.

Figure 5.1(continued): Loss of Nanchung or Inactive completely abolishes generator currents.

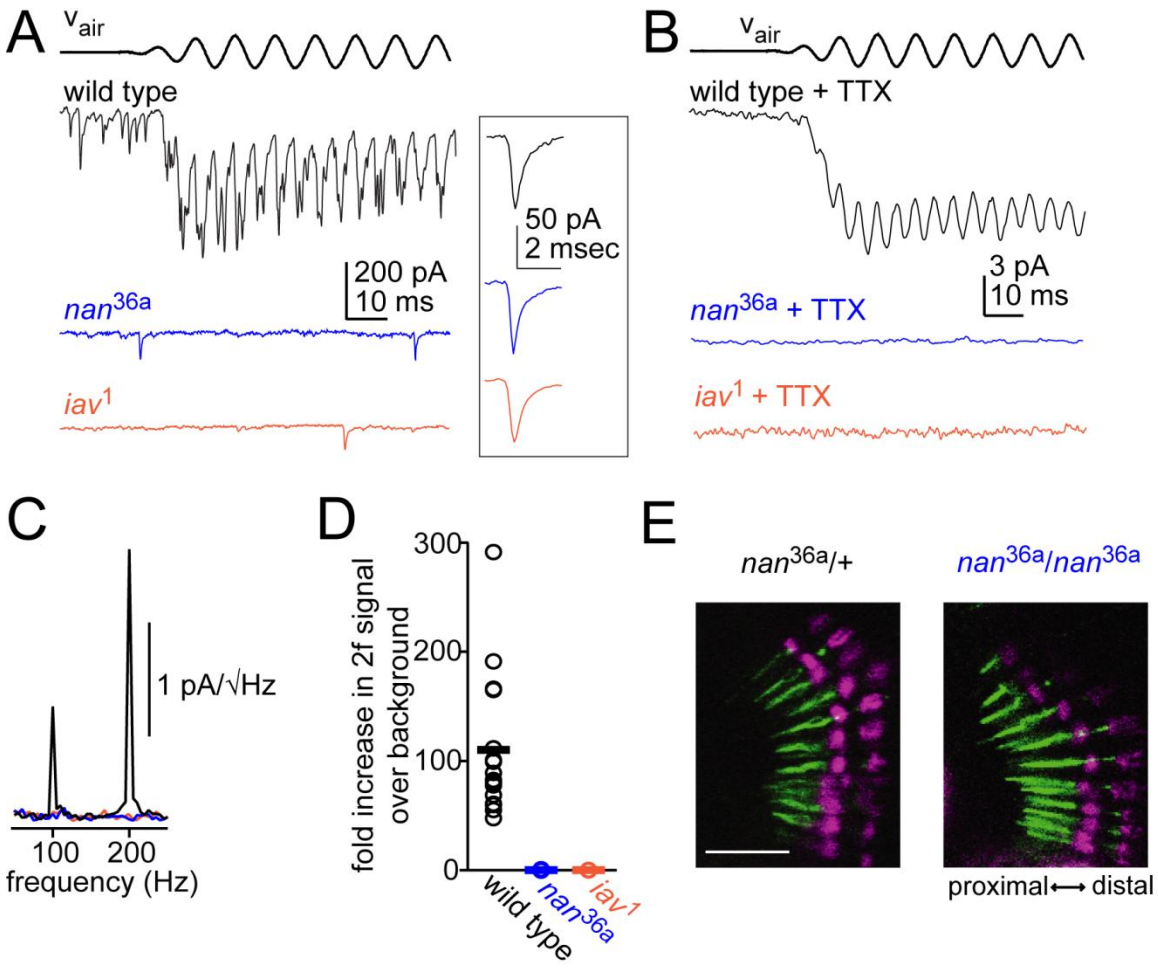

We observed no sound-evoked generator current in either mutant at any sound intensity in our test set. The strength of this observation depends critically on the sensitivity of our measurement, so we examined the recorded currents in the frequency domain where we expect signal detection to be optimal. The frequency representation shows a prominent peak at twice the frequency of the sound stimulus in wild type recordings, but there is no corresponding peak in recordings from the TRPV mutants at this frequency (Figure 5.1C). Focusing on a narrow band around this frequency, we calculated the signal gain over background noise for the currents recorded in TTX. On average, the signal gain was >110-fold in wild type, and indistuinguishable from zero in both mutants (Figure 5.1D). If the role of Nanchung and Inactive is simply to amplify the transduction signal, then they would need to amplify that signal at least 110-fold. If NompC is the transduction channel, one might imagine that these phenotypes could arise if NompC were trafficked improperly in these mutants; however, we confirmed that NompC localizes correctly even in the absence of Nanchung (Figure 5.1E). For these reasons, it seems more likely that Nanchung and Inactive form part of the transduction complex itself, or are required for proper trafficking of the transduction complex, rather than merely amplifying the transduction signal.

Loss of NompC decreases the sensitivity of generator currents to antennal rotation

We next examined generator currents in a *nompC* null mutant (nompC3; Tracey et al., 2003). In contrast to a previous report that used calcium imaging to monitor JON activity (Effertz et al.,

2011), we found that sound responses persist in the GFN recordings in these mutants, meaning that transduction is still present in type AB JONs. However, currents evoked by sound stimuli are systematically smaller in the mutants (Figure 5.2A). Sound-induced antennal rotations are also smaller in *nompC* mutants at some of these particle velocities due to a loss of active amplification (data not shown; see also Gopfert et al., 2006), so we controlled for this by measuring sound-evoked antennal movements in wild type flies and mutants, and plotting the sound response data in this frame of reference. This showed that currents in *nompC* mutants are smaller even if we control for the size of antennal rotations (Figure 5.2B). This phenotype is consistent across a range of sound frequencies. This implies that the loss of NompC reduces the sensitivity of the transduction complex to antennal rotation, a phenotype which is distinct from the effect of the mutation on antennal rotation.

The maximal amplitude of sound-evoked currents we recorded in *nompC* mutants is close to wild-type levels (Figure 5.2B). However, *nompC* responses to sound stimuli did not saturate, and so the true maximum amplitude is not clear from these recordings. Therefore, we extended our observations by measuring generator currents while using a rigid, piezoelectrically-actuated probe to rotate the antenna. In this recording configuration, step rotations produce short-latency currents which decay over tens of milliseconds; the rapid adaptation to the static step is further evidence that the GFN is postsynaptic to the fast-adapting AB JONs and not the slow-adapting CE JONs (Kamikouchi et al., 2009). Step rotations of the antenna produce currents which increase monotonically with step amplitude and saturate for the largest steps (Figure 5.2C,D).

In the *nompC* mutants, responses to small steps are systematically weaker as compared to wild type (Figure 5.2C, D). For small steps, the rise time is also slower in the *nompC* mutant than in wild type. In effect, mutant responses look like wild type responses to smaller steps,

suggesting that the transduction complex is experiencing less force than normal. Importantly, however, the maximal amplitude of step responses is similar for wild type and *nompC* mutants (Figure 5.2D), and in these responses the kinetics are also similar (Figure 5.2E). These results imply that NompC does not alter properties inherent to the transduction channels (maximum conductance, kinetics) or produce an additional conductance with distinct properties. Rather, NompC is required for normal sensitivity of the transduction complex to antennal movement.

Figure 5.2: Loss of NompC decreases the sensitivity of generator currents to antennal rotation.

(A) Generator currents recorded in response to sound stimuli (100 Hz tones at 0.00034, 0.0024, 0.011 m/sec). The particle velocity fluctuations from the weakest sound stimulus cannot be seen on this scale. Traces are averaged across all cells recorded in each genotype (n=9 wild type, 6 nompC3). (Note that currents in nompC mutants oscillate at the sound frequency, in contrast to wild type currents that oscillate at twice this frequency; this is characterized in detail below.)

(B) Average generator currents plotted versus the amplitude of antennal rotations evoked by sound, for three sound frequencies (n=9 wild type, 6 nompC3).

(C) (top) Piezoelectric step stimuli (lateral steps producing rotations of 0.0007 - 0.047 radians), measured using laser Doppler vibrometry of the piezoelectric stack. (bottom) Generator currents recorded in wild-type and nompC mutants in response to a family of piezoelectric step rotations.

(D) Average peak generator currents elicited by a family of lateral rotation steps (n=8 wild type and 6 nompC3). For sub-maximal steps, responses in nompC mutants are smaller than wild type. However, the wild type and mutant response reach the same maximum amplitude.

(E) Average rise time of generator currents versus the amplitude of antennal rotations produced by the piezoelectric probe in the lateral direction. Overall, the rise times in nompC mutants are slower than wild type. However, the rise times are equivalent for the largest steps tested.

Figure 5.2 (continued): Loss of NompC decreases the sensitivity of generator currents to antennal rotation.

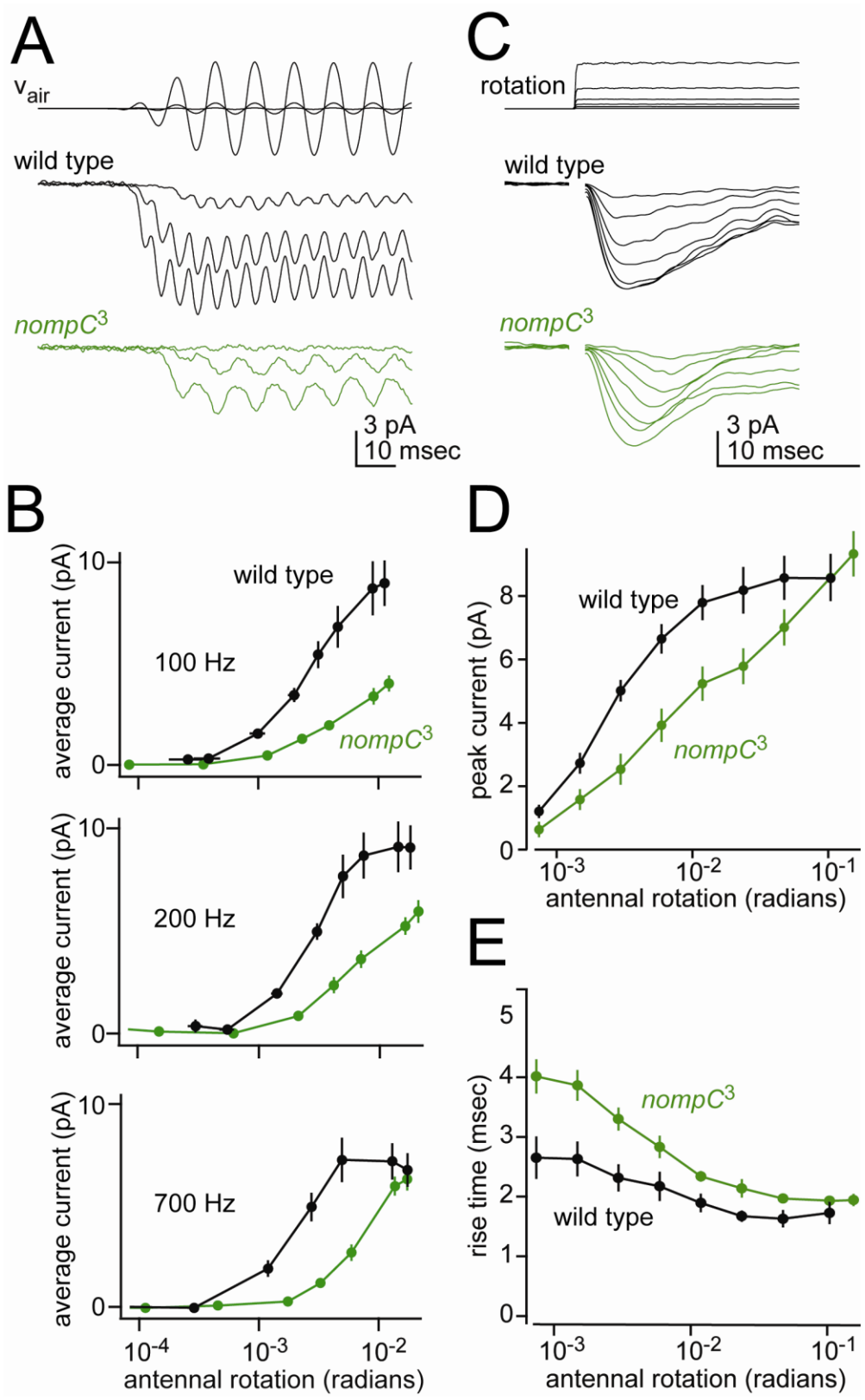

Loss of NompC leads to asymmetric transduction

Another notable feature of the *nompC* mutant phenotype is that mutant responses lack the symmetry of wild type responses. In wild type recordings, responses to medial and lateral steps are similar in magnitude and kinetics, and both the onset and offset of a step elicit a response (Figure 5.3A,B). This implies bidirectional and symmetric transduction in response to medial and lateral forces. (Bidirectional responses could reflect the existence of opponent populations of JONs (Kamikouchi et al., 2009; Kamikouchi et al., 2006; Yorozu et al., 2009). Alternatively, individual neurons could be bidirectionally responsive. In fact, our data argues that signals in the GFN are due to bidirectional transduction in a single opponent population of receptor neurons (Figure 5.4); however, none of the conclusions in this study rely on this idea.)

In *nompC* mutants, responses are still bidirectional, but responses to small medial steps are systematically smaller than responses to small lateral steps (Figure 5.3A-C). Indeed, the smallest medial steps often produce an outward current (rather than an inward current) in *nompC* mutants (Figure 5.3A), implying a decrease (rather than an increase) in transduction. If we define the "set point" as the antennal position that produces minimal transduction, then this means that the set point is matched to the antenna's resting position in wild type recordings, but is shifted from the antenna's resting position in the *nompC* mutant (Figure 5.3C). In addition, the difference between medial and lateral steps is more variable across recordings in the mutants than in wild type (Figure 5.3B), meaning that the position of the set point is more variable in the mutants.

Figure 5.3: Loss of NompC impairs the regulation of resting forces on the transduction complex.

(A) Generator currents evoked in response to a series of step rotations produced by the piezoelectric device (up to 0.012 radians, top). The small oscillations in the wild type recording after the step are due to resonant movements of the piezoelectric probe mounting arm, which are recorded in the laser Doppler vibrometer measurement of probe displacement but are not discernable at this scale. These responses reflect the high sensitivity of the wild type response.

(B) Histograms showing the magnitude of the response asymmetry (peak lateral response – peak medial response for the same step) for the 5 smallest steps in our test set. The mean of the wild-type distribution is not significantly different from 0, the value corresponding to no asymmetry (Wilcoxon test, $p=0.18$). The mean of the nompC mutant distribution was significantly different than 0, indicating a lateral bias (Wilcoxon test, $p<0.001$, $n=8$ wild type, $n=11$ nompC3). In addition, the variance of the wild type and mutant distributions are not equal (Levine's test for homogeneity of variance, $p<0.0001$). The mutant responses become more symmetric for larger steps.

(C) Peak generator currents recorded in wild type and nompC mutant flies in response to small steps. In wild type flies, the "set point" (i.e., the point of minimum current) matches the resting position of the antenna. In mutant recordings, it is shifted medially.

(D) Representative generator currents recorded in wild type and nompC mutant flies in response to sound (100 Hz tone, 0.0043 m/sec). A sound stimulus of this intensity produces antennal movement of similar amplitude in both genotypes (3.9 and 4.1 milliradians in nompC3 and wild type, respectively). However, wild type generator currents oscillate at twice the sound frequency (2f), whereas mutant currents oscillate mainly at the sound frequency (1f).

(E) Group data showing signal strength in the generator currents at 1f and 2f for wild type and nompC mutants (same stimulus as in E). In the nompC mutant, note that the 2f signal is relatively small, although still several-fold larger than the signal at surrounding frequencies. Some 2f signal is present in the nompC mutant at higher intensities: at the loudest sound intensity (0.015 m/sec), the 2f signal grows to about 20% of the 1f signal.

Figure 5.3 (continued): Loss of NompC impairs the regulation of resting forces on the transduction complex.

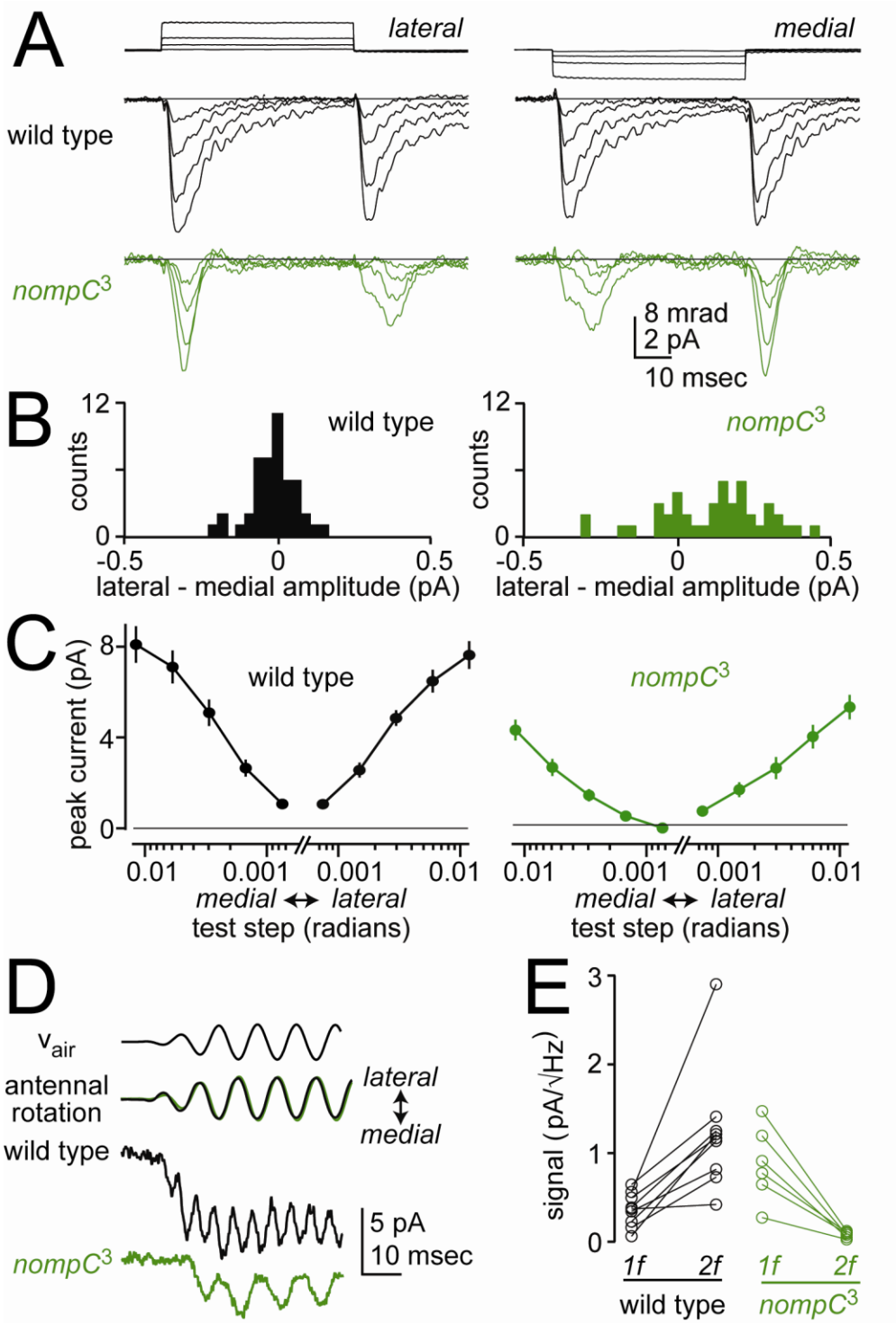

This asymmetry in responses to step stimuli has an obvious parallel in responses to sound stimuli. In wild type recordings, sound elicits oscillations in the generator current at twice the sound frequency (Figure 5.3D, E), consistent with symmetric and bidirectional responses to each sound cycle. By contrast, in *nompC* mutants, sound elicits oscillations predominantly at the sound frequency, with a smaller response at twice that frequency (Figure 5.3D, E). Like the responses to the piezoelectric probe, responses to sound-evoked antennal movement are substantially smaller in the medial direction as compared to the lateral direction.

Figure 5.4: Signals in the GFN likely reflect bidirectional transduction in one opponent population of JONs.

(A) Schematic cross-section through the second antennal segment (a2). When the third antennal segment (a3) rotates, the stalk of a3 alternately applies forces to two opponent populations of JONs. Shown here is one pair of JONs in each population. JON axons exit a2 to join the antennal nerve.

(B) Representative recordings of antennal rotation, antennal nerve field potential, and GFN generator current in wild type and the *nompC*^{3} mutant. Note the presence of a frequency doubled response in the field potential recording.

(C) Frequency-domain representations of the corresponding recordings. In response to a 100 Hz tone, the antenna rotates at the same frequency (1f). The dominant signal in the antennal nerve field potential is at twice this frequency (2f), likely reflecting the summed activity of both opponent populations of JONs. In contrast, the generator current recorded in the GFN in *nompC*^{3} mutants is predominantly at 100 Hz (1f). The loss of the 2f component in the generator current suggests that the GFN receives input from only one of the two opponent populations of JONs.

(D) Spike-mediated current in the GFN evoked by movements of the piezoelectric probe. Traces at top show the probe command, traces below show current averaged across multiple trials (no TTX). Test steps were applied before an adapting step, or else after an adapting step with delays of 6, 15, and 100 msec. The response to the adapting step is subtracted from the traces. Note that responses to the test step are inhibited shortly after the adapting step, regardless of whether the test step is in the same or opposite direction as the adapting step (black is lateral, magenta is medial).

(E) Group data showing spike-mediated current, normalized to the average test step response in each recording (mean +/- SEM, n = 3). The gray line shows the predicted response to medial steps (magenta) if JONs were unidirectionally gated. Instead, there is clear cross-adaptation between medial and lateral steps. Because spiking adaptation is a cell-autonomous process, this result suggests that individual JONs presynaptic to the GFN are activated by both medial and lateral steps. Together with (A), these data suggest that the GFN is connected to a single opponent population of JONs that is activated by both medial and lateral movements.

Figure 5.4 (continued): Signals in the GFN likely reflect bidirectional transduction in one opponent population of JONs.

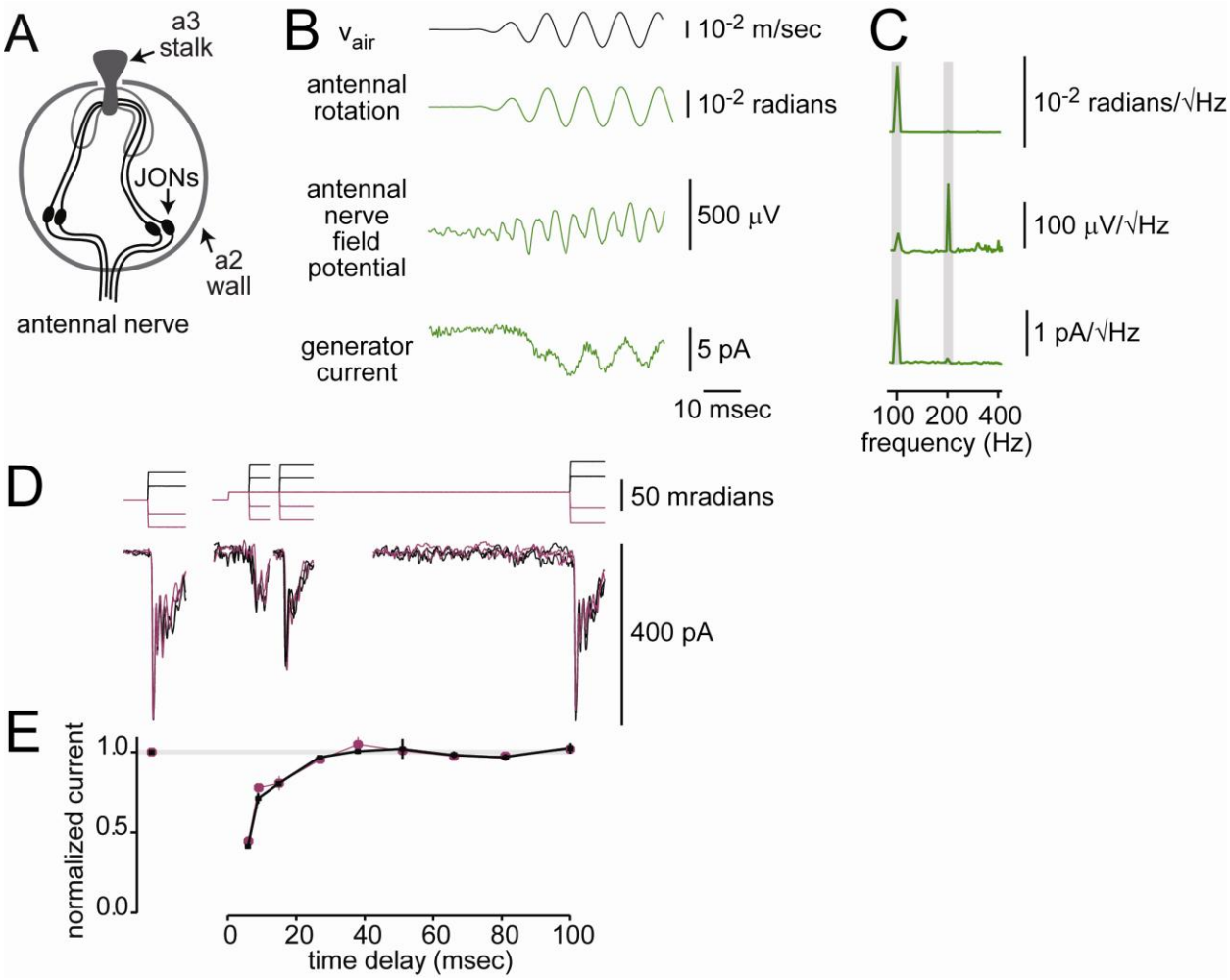

Loss of NompC does not prevent adaptation to static displacements

The antennae are subject to sustained forces in our recording environment; for instance, the gravitational field produces a constant force in the medial direction. Accordingly, we considered two explanations for the lateral bias we observe in the *nompC* mutant: either the bias is inherent

to the JONs, or else it reflects a failure to properly adapt to sustained forces. To investigate this, we used the piezoelectric probe to apply test steps of various amplitudes, either from a starting point corresponding to the antenna's resting position, or from a new starting point that was offset from the resting position. We chose an offset step that was large enough to evoke a nearly-saturating generator current (Figure 5.5A). Nevertheless, within <30 msec, currents had regained sensitivity to small displacements in both directions (Figure 5.5A,B). In other words, the region of maximal sensitivity to displacement was re-centered around the new static position (Figure 5.5B). This implies that the lateral and medial resting forces on the transduction complex have been re-equalized.

In *nompC* mutants, we observed the same process. Although the overall sensitivity of the system was lower in the mutants, the region of minimal transduction and maximal sensitivity still migrated by an amount that is equal to the magnitude and direction of the static offset (Figure 5.5C,D). These results demonstrate that the lateral bias in the *nompC* mutant is inherent to the JONs, and does not reflect an inability to adapt to a sustained force. These results also show that the *nompC* mutant is still capable of modulating the resting forces on the transduction complex. The key difference in the mutant is that this process of modulation occurs imprecisely, such that medial and lateral forces are chronically mismatched (Figure 5.4C), and the degree of matching is more variable across recordings (Figure 5.4B).

Figure 5.5: Loss of NompC does not prevent adaptation to static forces.

(A) A test step with the piezoelectric probe evokes a transient generator current (left). Next, a static lateral adapting step is applied, followed 27 msec later by another test step to determine the effect of the adapting step (right). The adapting step is 0.01185 radians. Test steps displayed here range from 0.00074 radians to 0.04740 radians. Although the adapting step is large enough to produce a nearly-saturating transient current, JONs rapidly regain sensitivity to both lateral and medial test steps within 27 msec of the onset of the adapting step. Stimulus artifacts are blanked.

(B) Group data showing peak current averaged across all experiments for each test step amplitude, with and without the adapting step (n=7). The arrow above the x-axis denotes the size and magnitude of the adapting step. Note that the set point of the system adapts to the new position of the antenna by the amount of the static offset. (Inset shows the response to small steps on a logarithmic and expanded horizontal scale centered around the new resting position of the antenna.The two curves were measured measured 27 msec and 81 msec after the adapting step.)

(C-D) Same as above, but for nompC mutant recordings (n=11). Here the adapting step was larger (0.04740 radians) in order to elicit a response to the adapting step that was closer to the wild type response. The range of test step amplitudes was also extended, again due to the lower overall sensitivity of the mutant responses. Just as in wild type recordings, the region of maximum sensitivity moves to the new static position. (Inset shows that the medial-lateral asymmetry is preserved after the adapting step.)

Figure 5.5 (continued): Loss of NompC does not prevent adaptation to static forces.

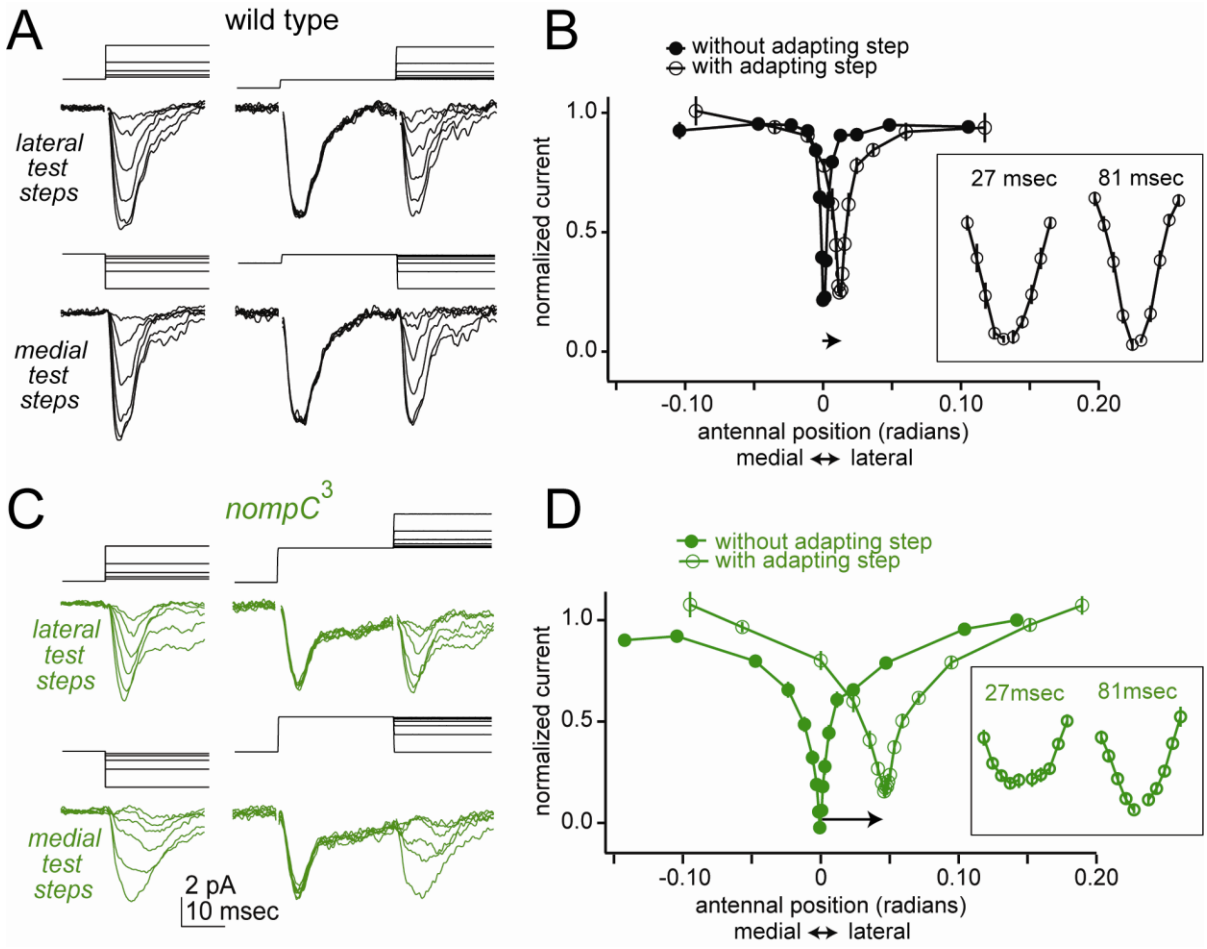

Loss of NompC disrupts alterations in the rotation-transduction curve during prolonged stimulation

An alternative way to modulate transduction is to stimulate the antenna with prolonged tone. This stimulus elicits changes in the generator current over the course of many cycles. In wild type recordings, three changes are prominent (Figure 5.6A). First, the total sound-evoked current declines over time. Second, the size of the sound-locked phasic oscillations also declines. Third, sound offset reveals an inward current which decays slowly (the "tail current").

Figure 5.6: Loss of NompC disrupts changes in transduction during prolonged stimulation.

(A) Sound-evoked generator currents in wild type, nompC hypomorphs (nompCf00642/nompC3), and nompC3 (null) homozygotes for 200 Hz and 100 Hz tones (intensity 0.0059 and 0.0044 m/sec, respectively). Total sound-evoked current decays after sound onset (magenta single arrow). In addition, the sound-evoked phasic oscillations decay (double-headed arrows). Finally, sound offset produces a tail current (open arrowhead). In the nompC3 homozygote, the decay in total current is still present. However, the tail current is absent and the decay in the amplitude of the phasic oscillations is reduced. The hypomorph has an intermediate phenotype.

(B-D) Group data averaged across experiments (n=9 wild type, 8 hypomorphs, 10 homozygotes). The nompC3 homozygotes are significantly different from wild type with respect to the average decay in the amplitude of phasic oscillations ($p<10^{-8}$), and average amplitude of the tail current ($p<0.005$, t-tests). There is no significant difference in the decay of the total current.

(E) Model schematic showing a rapid outward shift of the two transduction-displacement curves (top) and the simulated current produced by a model that incorporates this process (bottom). The input to the model is a ramped sinusoidal displacement (black line). The outward shift in the curves produces a rapid decay in the total current, together with a notch in the current after sound offset.

(F) Model schematic showing an initially uniform population of curves that are slowly shifted outward or inward to variable degrees (top). The simulated current (bottom) displays a slow decay in the amplitude of phasic oscillations, together with a tail current after sound offset.

(G) Model schematic showing a set point that is displaced from the resting position of the antenna (top). The simulated current (bottom) displays a larger resting current, and a loss of frequency-doubling.

(H) Simulated current where the population of curves rapidly shifts outward after tone onset, then slowly becomes more variable in the amount of shift over the course of the stimulus. After stimulus offset, the population shifts inward and then becomes less variable. This simulation recapitulates the key kinetic features of the wild type data.

(I) The simulated current produced by a population of curves that begin with high variability and have an average set point displaced from zero. The curves shift outward during stimulation, and then back inward after stimulus offset, but the variability never changes. This simulation recapitulates the key kinetic features of the nompC3 homozygote data.

(J) The simulated current produced by a model where all parameters are exactly intermediate to the parameters in panels H and I. This simulation recapitulates the key kinetic features of the nompC hypomorph data.

Figure 5.6 (continued): Loss of NompC disrupts changes in transduction during prolonged stimulation.

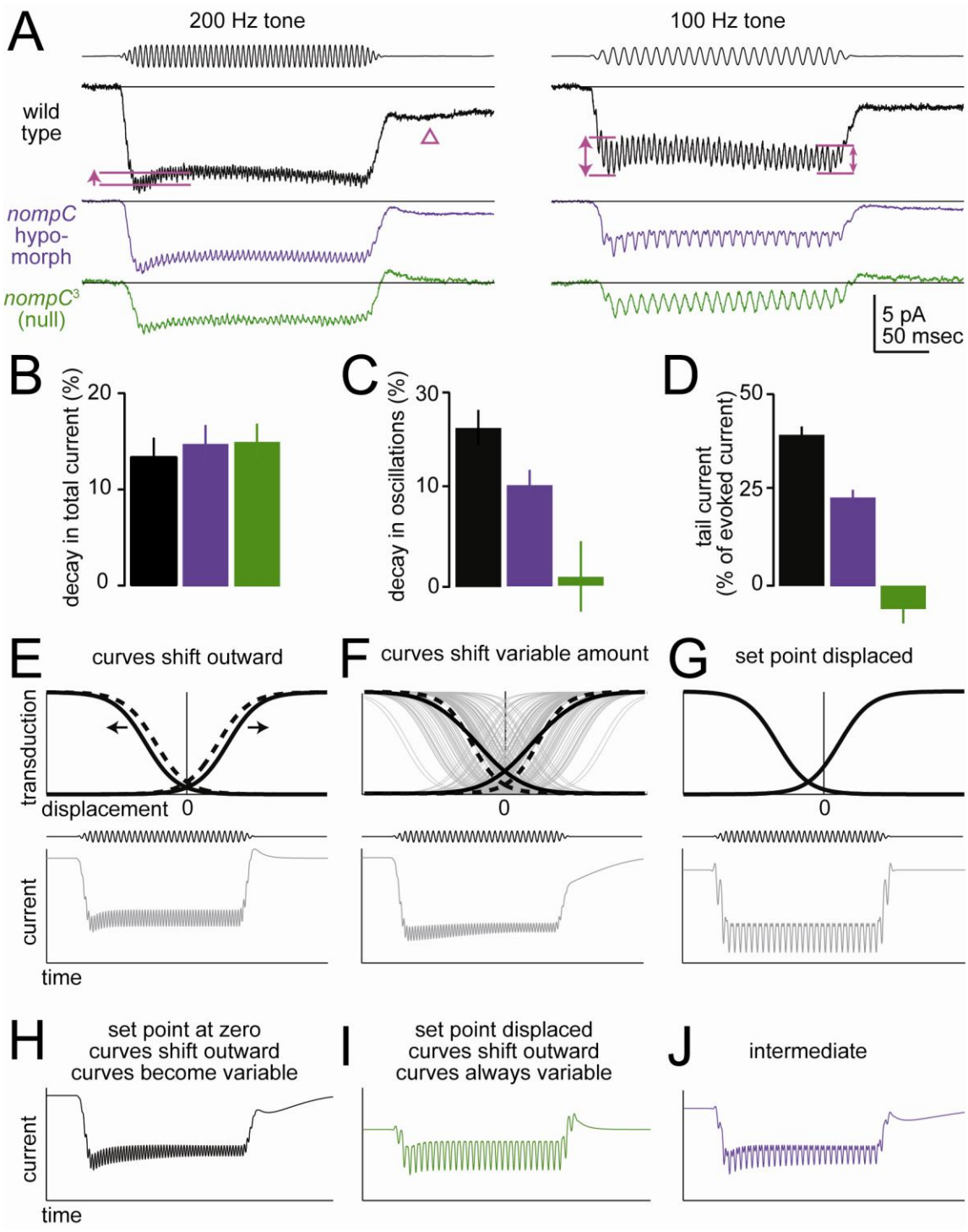

In *nompC* mutants, the total sound-evoked current declines over time, just as in wild type (Figure 5.6A,B). However, the decline in the sound-locked phasic oscillations is absent (Figure 5.6A,C). Also, at sound offset, there is no tail current (Figure 5.6A,D). Recordings from *nompC* hypomorphs showed a phenotype that is intermediate between *nompC* mutants and wild type (Figure 5.6A-D), implying that these dynamics depend quantitatively on the level of NompC protein.

Dynamics in the generator current imply changes in the transduction-displacement curves. There must be two such curves, corresponding to transduction induced by medial and lateral movements, respectively. The decline in total current over time (Figure 5.6B) can be accounted for by an outward shift in both curves (Figure 5.6E). This is similar to the shift induced by a static adapting step (Figure 5.5B), except that it occurs independently in the medial and lateral curves. This can be viewed as adaptation occurring in both directions in response to repetitive bidirectional displacements.

Next, we considered the decline in the size of the sound-locked phasic oscillations. This could occur if each curve is actually the sum of many individual curves (representing individual JONs or individual transduction channels) which shift by a variable amount over time (Figure 5.6F). Individual variability creates a summed curve with a flatter slope. This can explain not only the decline in the amplitude of the phasic oscillations, but also the tail current (Figure 5.6F).

We find that wild type responses can be fit by a model that combines these two processes: the individual curves shift to a variable degree, but on average they tend to shift outward. After tone offset, the individual curves shift inward and become more uniform again. This can be viewed as imprecise adaptation, followed by a process that restores the curves

precisely to their resting state. Currents simulated using this model show all the key kinetic features of wild type currents: frequency doubling, a decline in total current, a decline in the amplitude of phasic oscillations, and a tail current (Figure 5.6H).

The *nompC* mutant responses can be fit by a model that lacks this process of precise restoration. In this model, the curves are not centered properly at the antenna's resting position (Figure 5.6G), consistent with our data (Figure 5.3C). Moreover, the individual curves are positioned variably even in the resting state, giving rise to summed curves having a flatter slope, again consistent with our data (Figure 5.3B,C). The curves still shift outward during prolonged stimulation in this model, but high variability in the resting state occludes any further increase in variability during adaptation. Currents simulated using this model reproduce the key kinetic features of *nompC* mutant responses (Figure 5.6I): there is little frequency-doubling in the phasic oscillations (because the summed curves have a set point which is displaced from zero), little decline in the phasic oscillations (because the summed curves do not flatten), and no tail current (again, because the summed curves do not flatten). Note that the resting inward current generated by this model is larger than in the wild type model, consistent with the elevated spontaneous firing in *nompC* mutant recordings (Figure 5.7).

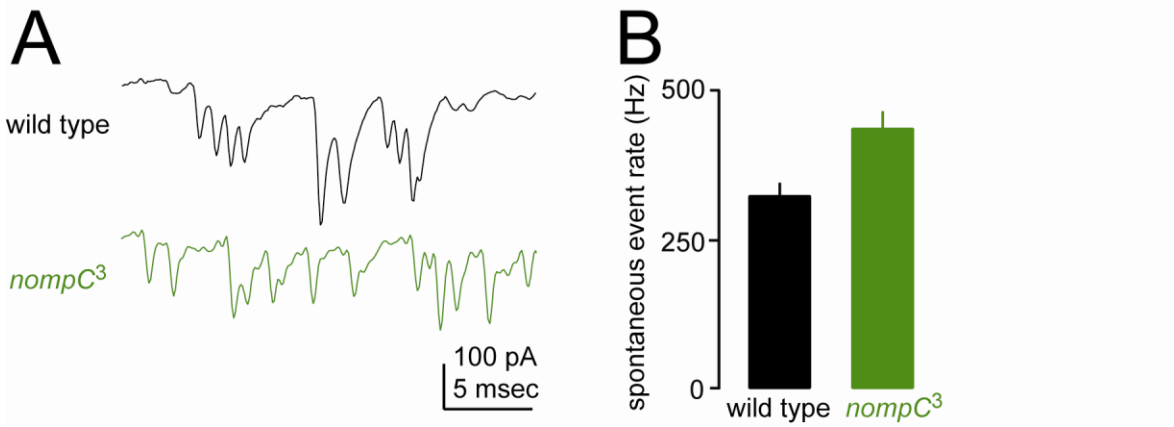

Figure 5.7: Spontaneous event rate is increased in nompC mutants.

(A) Representative recordings of spontaneous events (i.e., putative JON spikes, recorded from the GFN with TTX omitted from the bath) from a wild type neuron and a nompC mutant neuron.

(B) Group data averaged across recordings. Spontaneous event rate is significantly higher in the mutant ($p<0.01$, t-test, n=15 wild type, 12 nompC3). Also, events in wild-type tended to come in clusters, whereas inter-event intervals in the mutant were Poisson distributed.

Because loss of spontaneous events is correlated with loss of transduction (Figure 4A), spontaneous events likely reflect a basal level of transduction in the antenna's resting state. This is consistent with a model where the transduction-displacement curves are flatter and more asymmetric than wild type (Figure 5.7).

Finally, if we set all the parameters in the simulation to values exactly intermediate to these two cases, we obtain currents with intermediate properties (Figure 5.6J). This model can account for the appearance of the *nompC* hypomorph. This result suggests that the precision by which transduction-displacement curves are regulated depends on the amount of NompC protein.

Discussion

Properties of transduction in auditory receptor neurons

Our results illustrate several fundamental properties of transduction in *Drosophila* JONs. First, our measurements show that the transduction complex is gated by antennal rotations as small as 0.00076 radians. During this rotation, the distal end of the "lever" which projects from the antenna (called the arista) is displaced by 74 nm. The displacement that gates the transduction complex is certainly much smaller than this (on the order of a few nm), but because this displacement occurs within the interior of the antenna itself, we cannot measure it directly(Robert et al., 1996).

Second, our data argue that transduction in individual JONs is bidirectionally gated by both medial and lateral movements (Figure 5.3). Bidirectional responses have been described previously in mechanoreceptors. These include rapidly-adapting cutaneous mechanoreceptors (Pologruto et al., 2003) and some low-threshold mechanoreceptors (Ruta et al., 2010) in mammals, as well as *C. elegans* mechanoreceptors (Fischer et al., 1988; Kang et al., 2010; Phelan et al., 2008; Story et al., 2003). In general, the mechanisms of bidirectional responsiveness are poorly understood.

Finally, we find that there is basal transduction in JONs even in the absence of sound. This conclusion relies on our observation that JONs spike spontaneously, and that spontaneous activity is abolished by loss of either Nanchung or Inactive. This conclusion is consistent with previous studies which used other techniques to make inferences about JON activity (Kamikouchi et al., 2009; Robert et al., 1996).

TRPV family members as transduction complex components

Our findings are consistent with previous reports that loss of either Nanchung or Inactive completely eliminates antennal field potential responses to sound (Gong et al., 2004; Kim et al., 2003). However, these potentials are interpreted as reflecting the spiking activity of JONs rather than subthreshold activity (Xiang et al., 2010). Thus, it was not clear from this result whether Nanchung and Inactive were required for transduction or merely spike generation.

Our results go beyond previous work to demonstrate that Nanchung and Inactive are required for measurable generator currents in auditory receptor neurons. The transduction latency and speed of the generator currents we record implies that the transduction complex is directly gated by force, rather than being gated indirectly by a second messenger. Given this, the Nanchung/Inactive complex is unlikely to merely amplify a pre-existing transduction signal, because amplification would need to occur within microseconds (which rules out a role for diffusible second messengers), and amplification would need to be >100-fold in magnitude (which is unlikely given the weak voltage dependence of these channels; Gong et al., 2004; Kim et al., 2003). Finally, because the Nanchung/Inactive complex does not co-localize with NompC in the JON dendrite (Kung, 2005; Lee et al., 2010), no amplification mechanism could rely on direct protein-protein interactions between these components.

Given these considerations, it seems likely that Nanchung and Inactive form part of the transduction complex itself. Consistent with this conclusion, both Nanchung and Inactive confer calcium responses to hypo-osmotic stimuli in heterologous cells (Gong et al., 2004; Kim et al., 2003). Moreover, the *C. elegans* TRPV orthologs *ocr-2*, and *osm-9* are required for normal behavioral responses to nose touch (Datta et al., 2008; Tobin et al., 2002). However, more work will be needed to test the idea that Nanchung and Inactive function as force-gated ion channels.

An alternative possibility is that Nanchung and Inactive are required for the trafficking or function of an unknown channel.

Previous studies have shown that the loss of Nanchung or Inactive results in abnormally large sound-driven antennal movements, as well as spontaneous oscillatory movement in the absence of sound (Gopfert et al., 2006). Our results show that this phenotype goes hand-in-hand with loss of all measurable transduction in JONs (Figure 5.1, 5.8). Together, these findings imply that transduction in JONs inhibits the active amplification of antennal movements. The presence of active movements in the absence of transduction is also incompatible with the idea that the active amplification of antennal movement is a direct consequence of transduction channel gating.

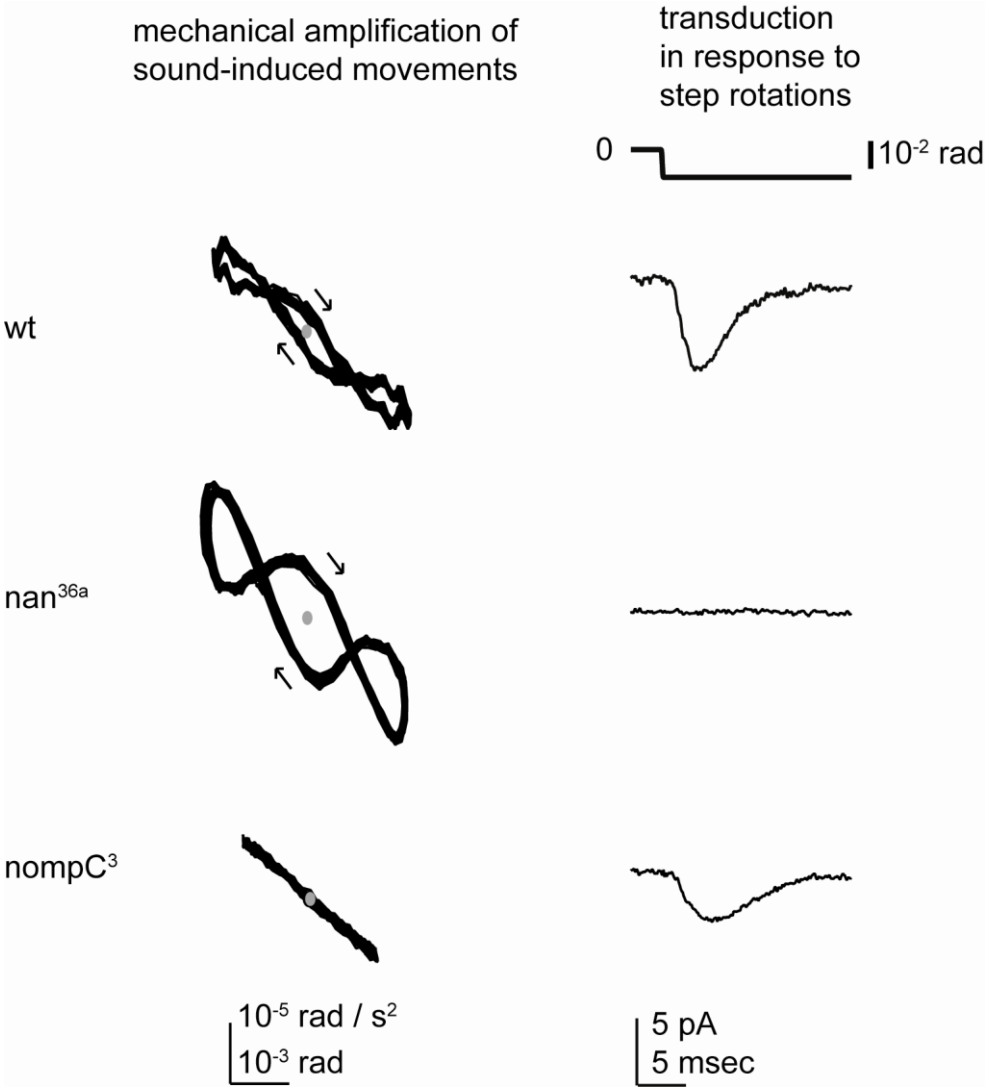

Figure 5.8: Active amplification and auditory transduction are separable in *Drosophila*.

(left) Phase plane plots of the antennal displacement versus acceleration during a sound stimulus for wild-type and mutant flies (200 Hz, 0.0059 m/sec). The linearization of the displacement-acceleration plot and smaller total angular displacement in the nompC mutant indicates the loss of a process that actively amplifies the antenna's mechanical response to sound. (right) Generator currents from wild type, and two TRP channel mutants. Transduction is absent in the nanchung mutant but present in the nompC mutant.

NompC as a modulator of mechanical forces

Our results demonstrate that NompC is not required for mechanotransduction in JONs. Indeed, the maximal level of transduction current is normal in the *nompC* mutant, and the kinetics of transduction are normal at this maximal level. This argues that NompC does not directly participate in the transduction complex. This result also makes it unlikely that NompC is required for the proper trafficking or localization of the transduction complex. There is no residual NompC-mediated current in the *nanchung* or *inactive* mutants, suggesting that NompC does not mediate an independent conductance. We cannot exclude the possibility of a NompC-mediated conductance which is too small for us to detect. Indeed a small calcium signal can be detected in *nanchung* mutant JONs in response to static deflection, although not in response to sound, and this measurement was not restricted to the type AB JONs (Kamikouchi et al., 2009).

To the extent that we can use the native mechanosensitive conductance as a force sensor, our results demonstrate that the role of NompC is to modulate the forces on the transduction complex, effectively amplifying the mechanical input to the transduction channel. On the basis of its subcellular location, NompC is well-positioned to serve this role. Whereas Nanchung/Inactive are localized to the proximal dendrite, NompC is localized to the distal dendrite, closer to the point where the dendrite inserts into the connective structures that link it to the moving segment of the antenna (Kung, 2005; Lee et al., 2010). A bundle of microtubules runs longitudinally through the dendrite (Koto et al., 1981), and this could provide a substrate for adjustments of tension that propagate from the distal to the proximal dendrite.

A previous study concluded that NompC is absolutely required for transduction in type AB JONs, on the basis of the finding that loss of NompC produces loss of movement-evoked

calcium signals in these JONs (Effertz et al., 2011). Several lines of evidence demonstrate that we are selectively monitoring type AB JONs, and so the basis for this discrepancy is not clear. Resting transduction appears to be increased in the *nompC* mutant (Figure 5.7), and a corresponding increase in intracellular calcium could reduce the sensitivity of the high-affinity calcium indicator used to report JON activity in the previous study.

Previous studies have shown that loss of NompC abolishes active amplification of sound-evoked antennal movement, as well as inhibiting spontaneous oscillatory antennal movement (Gopfert et al., 2006; Gopfert and Robert, 2003). Thus, loss of NompC appears to eliminate or occlude a process that exerts force on the antennal receiver. This is consistent with our conclusion that NompC is a modulator of forces within the auditory organ.

Future studies will be needed to clarify the molecular mechanism of NompC's action in JONs. In one hypothetical scenario, NompC functions as a channel, and ionic flux through this channel is permissive for a process that adjusts the longitudinal tension within the JON. If so, then this ionic flux must carry at least 110-fold less charge than the charge that flows through the transduction complex itself. This is a plausible scenario if NompC were preferentially permeable to calcium over other cations. Alternatively, NompC may not be electrogenic at all. Rather, the putative pore domain (which is not conserved in *Drosophila*; Kang et al., 2010) might have lost its ion conducting property, and another domain of the protein might act directly as a mediator or modulator of force generation, similar to the role of prestin in outer hair cells. NompC contains an unusually large number of ankyrin repeats, which can act as elastic elements, and can generate a re-folding force when unfolded (Anderson et al., 1991; Chung et al., 2008).

Chapter 6

Conclusion

The experiments described here detail our efforts to identify neurons within the Drosophila auditory system and studies of the mechanism of transduction in the primary auditory neurons. Using the technique described in Chapter 4, we have recorded generator currents from the primary auditory neurons in wild type and TRP channel mutant animals. On the basis of our data, we find that:

1. The *Drosophila* neural sound threshold is approximately 55 dB SVL for pure tones at the antenna's resonant frequency. This is orders of magnitude higher than the threshold for the active process, indicating that transduction and active amplification may be separable.

2. The TRPV channels Nanchung and Inactive are members of the transduction complex and required for generator currents. They are the most likely candidates for the Drosophila auditory transduction channel(s).

3. NompC modulates the forces on the transduction complex at rest and during a sound stimulus, and NompC is quantitatively required for maintaining symmetric transduction to lateral and medial antennal deflections.

4. The *wild type* and *nompC* mutant adapt to sustained antennal displacements. An outward shift in the rotation transduction curve to a symmetric sound stimulus suggests that the rate of adaptation to outward movements exceeds that of inward movements, a phenomena also observed in vertebrate hair cells. In *wild type*, a tone stimulus also produces an apparent

flattening of the rotation-transduction curve, implying jitter in the rate of adaption across individual transducer elements. This process is absent in the *nompC* mutant suggesting the absence of a mechanism that harmonizes the state of adaptation across the tranducer population.

5. Active amplification and transduction are genetically separable in *Drosophila*, as only one of these processes is preserved in the TRPV and TRPN1 mutants, respectively. This is in contrast to models of active hair bundle movement, which invoke changes in the gating state of the transducer channel.

The sensitivity of the *Drosophila* auditory system

Two processes specify the sensitivity of the Drosophila auditory system to sound. The first, described by Gopfert and colleagues, is an apparent frequency-dependent active amplification of antennal movement. The estimated power gain of the active process produces a ~10-fold increase in the movement of the antenna in response to weak sounds(Gopfert et al., 2006). A second mechanism is uncovered in the *nompC* mutant, which shows an ~3-fold shift in the rotation-transduction relationship (see Chapter 5). Together, these processes render the wild type antenna ~30 fold more sensitive to sound relative to flies lacking NompC. It may be that that NompC mediates both sensitization processes through its role in active amplification. For instance, NompC might somehow sense the antenna's position and be required for a force that increases that antenna's displacement in response to sound while simultaneously increases the force on the transduction complex. On the other hand, NompC could serve an indirect, permissive role, such that the lack of active amplification in the *nompC* mutant may reflect a breakdown in the regulation of force at rest.

A model of force regulation in *Drosophila* auditory transduction

On the basis of our data, we propose a model of how forces on the transduction complex are regulated. In the normal auditory organ, transduction is gated by either lateral or medial movements of the antenna, and the position of maximal sensitivity to movement is the resting position of the antenna. This implies that medial and lateral forces on transduction channels are normally balanced. Loss of NompC disrupts this balance, suggesting that the ability of the system to precisely adjust the resting forces on the transduction complex has been lost.

Adaptation produces a re-balancing of medial and lateral forces. This is clear from the observation that a static deflection produces currents which decay rapidly, and it also shifts the point of maximal sensitivity to the new resting position of the antenna. Re-balancing medial and lateral forces would correspond to a concerted medial or lateral shift in both of the two transduction-displacement curves. Conversely, we observe that a prolonged tone stimulus appears to produce adaptation in both directions: the system behaves as if the response to medial movement adapts in the medial direction, while the response to lateral movement adapts in the lateral direction. This would correspond to both transduction-displacement curves shifting outward. Our results show that these basic adaptation processes are intact even when NompC is absent.

However, during the prolonged tone, adaptation is not perfect: the system behaves as if the slope of both curves becomes flatter over time. A flatter curve could reflect variability in the degree of adaptation across individual neurons or individual channels – in other words, imprecision in adaptation. After sound offset, the system behaves as if the many individual

neurons or channels were precisely restored to the same position. In the *nompC* mutant, the system behaves as if there is a defect in the process that precisely restores the individual transduction-displacement curves to the proper resting position.

Adaptation to static displacements is a well-known property of mechanotransduction. Interestingly, the transduction-displacement curves of hair cells also change their shape after adaptation (Crawford and Fettiplace, 1981; Nakai and Ohkura, 2003). This may reflect a conceptually similar process to what we have observed in *Drosophila* JONs, although the underlying mechanisms could be different.

Concluding remarks and future directions

The ionic basis for the auditory receptor potential was first recorded thirty years ago, yet the molecular identity of the auditory transduction channel is not known in any species (Corey, 2006; Corey and Hudspeth, 1979). In marked contrast, many species of voltage and ligand gated ion channels have been cloned and functionally reconstituted in heterologous expression systems in the last three decades. This had led to the examination of their structure through x-ray crystallography and modeling, and beautifully detailed studies of the mechanism of their gating at the level of single channel proteins. It is reasonable to hope that molecular identification of auditory transduction channels might mark the beginning of a similiarly fruitful period for the field of mechanosensation, which remains one of the least understood senses at the molecular level.

As part of this effort, we demonstrate that the TRPV channels Nanchung and Inactive are required for the auditory receptor potential in *Drosophila*. However, it is possible that these ion

channels are not themselves the transduction channel, but rather are required for the proper localization or function of other, unidentified channel proteins. One strategy for distinguishing between these possibilities would be to introduce versions of the TRPV channels with altered pore domains. Well-designed alterations in the pore of an ion channel can change the ionic selectivity and conductance of the channel without rendering it non-conducting. If mutations to the putative pore of an ion channel alter the conductance of the native current, this is taken of evidence that the ion channel is a pore-forming subunit of that conductance (Anderson et al., 1991; Kang et al., 2010). In experiments designed to determine the presynaptic inputs to the Giant Fiber Neuron, we rescue transduction in *inactive* null mutants through transgenic restoration of wildtype *inactive*, demonstrating the feasibility of this approach. It is important to note that there is evidence that the ionic selectivity of TRPV1 and other ion channels can vary with the degree of activation (Chung et al., 2008; Rosenmund et al., 1998). Thus, it may be difficult to disambiguate a change in ionic selectivity from a change in the degree of activation by a stimulus, which is not an intrinsic property of the channel pore.

We identify a role of TRPN1 in specifying the resting forces on the transduction channel, but do not determine the mechanistic basis of this phenotype. Importantly, we do not know the identities of the molecules that form the mechanical link between the antenna and the transduction apparatus, nor do we understand precisely how they might shape the forces that act on the transduction complex. Immuno-electron microscopy allows visualization of components of the mechanotransduction complex and cytoskeletal structures involved in channel gating, but this technique lacks the resolution required to produce a model of how mechanical force is shaped by intracellular and extracellular structures (Cueva et al., 2007). It is also unclear how exactly the channels themselves are gated by the forces produced by the sound field. Gating of

the hair cell transduction channel requires an extracellular tether, termed the tip-link, but it is not known is an analogous structure exists in the Johnston's Organ Neuron.

The fruit fly *Drosophila melanogaster* is an important model organism that has provided the basis for contributions to many fields of study, such as the function neural circuits, development, and immunity. However, it is natural to question the degree of correspondence between vertebrate hair cell and *Drosophila* auditory transducers. Superficially, they seem to have little relation to one another. For instance, the mechanical sound receivers differ in their structure and kinematics. They are sensitive to different aspects of the sound field, and perceive near and distant sounds differently. Finally, the ultrastructure of the fly primary auditory neurons bears a much stronger resemblance to the Pacinian corpuscle than the vertebrate hair cell. Yet the function of the Drosophila "ear" is analogous in many ways to that of vertebrates, showing an active process that increases sensitivity, spontaneous fluctuations in the absence of sound, adaptation to sustained displacements, and rapid transduction. Just as investigations into the function of voltage-gated channels and ligand-gated receptors have benefited enormously from techniques permitting the functional examination of mutant forms, the relative ease of genetic manipulation in *Drosophila* may make it particularly well-suited to *in vivo* studies of the role of transducer molecules in the sensation of sound.

Bibliography

Anderson, M.P., Gregory, R.J., Thompson, S., Souza, D.W., Paul, S., Mulligan, R.C., Smith, A.E., and Welsh, M.J. (1991). Demonstration that CFTR is a chloride channel by alteration of its anion selectivity. Science *253*, 202-205.

Armstrong, J.D., Texada, M.J., Munjaal, R., Baker, D.A., and Beckingham, K.M. (2006). Gravitaxis in Drosophila melanogaster: a forward genetic screen. Genes Brain Behav *5*, 222-239.

Art, J.J., Crawford, A.C., and Fettiplace, R. (1986). Electrical resonance and membrane currents in turtle cochlear hair cells. Hear Res *22*, 31-36.

Bennet-Clark, H.C. (1971). Acoustics of Insect Song. Nature *234*, 255-259.

Bennet-Clark HC, E.A. (1967). Stimuli provided by courtship of male *Drosophila melanogaster*. Nature *215*, 669-671.

Bennet-Clark, H.C., and Ewing, A.W. (1969). Pulse interval as a critical parameter in the courtship song of Drosophila melanogaster. Animal Behaviour *17*, 755-759.

Boekhoff-Falk, D.F.E.a.G. (2007). Development of Johnston's organ in Drosophila. Int J Dev Biol *51*, 679 - 687.

Card, G., and Dickinson, M.H. (2008). Visually mediated motor planning in the escape response of Drosophila. Curr Biol *18*, 1300-1307.

Chung, M.K., Guler, A.D., and Caterina, M.J. (2008). TRPV1 shows dynamic ionic selectivity during agonist stimulation. Nat Neurosci *11*, 555-564.

Corey, D.P. (2006). What is the hair cell transduction channel? J Physiol *576*, 23-28.

Corey, D.P., and Hudspeth, A.J. (1979). Ionic basis of the receptor potential in a vertebrate hair cell. Nature *281*, 675-677.

Coste, B., Mathur, J., Schmidt, M., Earley, T.J., Ranade, S., Petrus, M.J., Dubin, A.E., and Patapoutian, A. (2010). Piezo1 and Piezo2 are essential components of distinct mechanically activated cation channels. Science *330*, 55-60.

Crawford, A.C., and Fettiplace, R. (1981). An electrical tuning mechanism in turtle cochlear hair cells. J Physiol *312*, 377-412.

Crossley, S.A., Bennet-Clark, H.C., and Evert, H.T. (1995). Courtship song components affect male and female Drosophila differently. Animal Behaviour *50*, 827-839.

Cueva, J.G., Mulholland, A., and Goodman, M.B. (2007). Nanoscale organization of the MEC-4 DEG/ENaC sensory mechanotransduction channel in Caenorhabditis elegans touch receptor neurons. J Neurosci *27*, 14089-14098.

Curtin, K.D., Zhang, Z., and Wyman, R.J. (2002). Gap junction proteins expressed during development are required for adult neural function in the Drosophila optic lamina. J Neurosci *22*, 7088-7096.

Datta, S.R., Vasconcelos, M.L., Ruta, V., Luo, S., Wong, A., Demir, E., Flores, J., Balonze, K., Dickson, B.J., and Axel, R. (2008). The Drosophila pheromone cVA activates a sexually dimorphic neural circuit. Nature *452*, 473-477.

Drapeau, M.D., Radovic, A., Wittkopp, P.J., and Long, A.D. (2003). A gene necessary for normal male courtship, yellow, acts downstream of fruitless in the Drosophila melanogaster larval brain. Journal of Neurobiology *55*, 53-72.

Eberl, D.F., Hardy, R.W., and Kernan, M.J. (2000a). Genetically similar transduction mechanisms for touch and hearing in Drosophila. J Neurosci *20*, 5981-5988.

Eberl, D.F., Hardy, R.W., and Kernan, M.J. (2000b). Genetically Similiar Transduction Mechanisms for Touch and Hearing in *Drosophila*. J Neurosci *20*, 5981-5988.

Effertz, T., Wiek, R., and Gopfert, M.C. (2011). NompC TRP channel is essential for Drosophila sound receptor function. Curr Biol *21*, 592-597.

Ewing, H.C.B.-C.a.A.W. (1967). Stimuli provided by Courtship of Male *Drosophila melanogaster*. Nature *215*, 669 - 672.

Fischer, J.A., Giniger, E., Maniatis, T., and Ptashne, M. (1988). GAL4 activates transcription in Drosophila. Nature *332*, 853-856.

Geffeney, S.L., Cueva, J.G., Glauser, D.A., Doll, J.C., Lee, T.H., Montoya, M., Karania, S., Garakani, A.M., Pruitt, B.L., and Goodman, M.B. (2011). DEG/ENaC but not TRP channels are the major mechanoelectrical transduction channels in a C. elegans nociceptor. Neuron *71*, 845-857.

Gong, Z., Son, W., Chung, Y.D., Kim, J., Shin, D.W., McClung, C.A., Lee, Y., Lee, H.W., Chang, D.J., Kaang, B.K., *et al.* (2004). Two interdependent TRPV channel subunits, inactive and Nanchung, mediate hearing in Drosophila. J Neurosci *24*, 9059-9066.

Gopfert, M.C., Albert, J.T., Nadrowski, B., and Kamikouchi, A. (2006). Specification of auditory sensitivity by Drosophila TRP channels. Nat Neurosci *9*, 999-1000.

Gopfert, M.C., and Robert, D. (2001). Biomechanics: Turning the key on Drosophila audition. Nature *411*, 908-908.

Gopfert, M.C., and Robert, D. (2002a). The mechanical basis of Drosophila audition. J Exp Biol *205*, 1199-1208.

Gopfert, M.C., and Robert, D. (2002b). The mechanical basis of Drosophila audition. J Exp Biol *205*, 1199-1208.

Gopfert, M.C., and Robert, D. (2003). Motion generation by Drosophila mechanosensory neurons. Proc Natl Acad Sci U S A *100*, 5514-5519.

Hall, J.C. (1994). The Mating of the Fly. Science *264*, 1702 - 1714.

Hoy, G.S.P.R.R. (1979). Temporal Pattern as a Cue for Species-Specific Calling Song Recognition in Crickets. Science *204*, 429-432.

Hudspeth, A.J. (2008). Making an effort to listen: mechanical amplification in the ear. Neuron *59*, 530-545.

Kamikouchi, A., Inagaki, H.K., Effertz, T., Hendrich, O., Fiala, A., Gopfert, M.C., and Ito, K. (2009). The neural basis of Drosophila gravity-sensing and hearing. Nature *458*, 165-171.

Kamikouchi, A., Shimada, T., and Ito, K. (2006). Comprehensive classification of the auditory sensory projections in the brain of the fruit fly Drosophila melanogaster. J Comp Neurol *499*, 317-356.

Kang, L., Gao, J., Schafer, W.R., Xie, Z., and Xu, X.Z. (2010). C. elegans TRP family protein TRP-4 is a pore-forming subunit of a native mechanotransduction channel. Neuron *67*, 381-391.

Kazama, H., and Wilson, R.I. (2008). Homeostatic matching and nonlinear amplification at identified central synapses. Neuron *58*, 401-413.

Kernan, M. (2007). Mechanotransduction and auditory transduction in <i>Drosophila</i&gt. Pflügers Archiv European Journal of Physiology *454*, 703-720.

Kernan, M., Cowan, D., and Zuker, C. (1994). Genetic dissection of mechanosensory transduction: mechanoreception-defective mutations of Drosophila. Neuron *12*, 1195-1206.

Kim, J., Chung, Y.D., Park, D.Y., Choi, S., Shin, D.W., Soh, H., Lee, H.W., Son, W., Yim, J., Park, C.S., *et al.* (2003). A TRPV family ion channel required for hearing in Drosophila. Nature *424*, 81-84.

Kim, S.E., Coste, B., Chadha, A., Cook, B., and Patapoutian, A. (2012). The role of Drosophila Piezo in mechanical nociception. Nature.

Koto, M., Tanouye, M.A., Ferrus, A., Thomas, J.B., and Wyman, R.J. (1981). The morphology of the cervical giant fiber neuron of Drosophila. Brain Res *221*, 213-217.

Kung, C. (2005). A possible unifying principle for mechanosensation. Nature *436*, 647-654.

Kyriacou, C.P., and Hall, J.C. (1984). Learning and memory mutations impair acoustic priming of mating behaviour in Drosophila. Nature *308*, 62-65.

Kyriacou CP, H.J. (1982). The function of courtship song rhythms in *Drosophila*. Animal Behavior *30*, 794 - 801.

Lee, J., Moon, S., Cha, Y., and Chung, Y.D. (2010). Drosophila TRPN(=NOMPC) channel localizes to the distal end of mechanosensory cilia. PLoS One *5*, e11012.

Lima, S.Q., and Miesenbock, G. (2005). Remote control of behavior through genetically targeted photostimulation of neurons. Cell *121*, 141-152.

Menda, G., Bar, H.Y., Arthur, B.J., Rivlin, P.K., Wyttenbach, R.A., Strawderman, R.L., and Hoy, R.R. (2011). Classical conditioning through auditory stimuli in Drosophila: methods and models. J Exp Biol *214*, 2864-2870.

Miller, D. (1979). Acoustic Basis of Mater Recognition by Female Zebra Finches. Animal Behavior *27*, 376-380.

Miyamoto, T., and Amrein, H. (2008). Suppression of male courtship by a Drosophila pheromone receptor. Nat Neurosci *11*, 874-876.

Nadrowski, B., Albert, J.T., and Gopfert, M.C. (2008). Transducer-based force generation explains active process in Drosophila hearing. Curr Biol *18*, 1365-1372.

Nakai, J., and Ohkura, M. (2003). Probing calcium ions with biosensors. Biotechnol Genet Eng Rev *20*, 3-21.

Pfeiffer, B.D., Jenett, A., Hammonds, A.S., Ngo, T.T., Misra, S., Murphy, C., Scully, A., Carlson, J.W., Wan, K.H., Laverty, T.R., *et al.* (2008). Tools for neuroanatomy and neurogenetics in Drosophila. Proc Natl Acad Sci U S A *105*, 9715-9720.

Phelan, P., Goulding, L.A., Tam, J.L., Allen, M.J., Dawber, R.J., Davies, J.A., and Bacon, J.P. (2008). Molecular mechanism of rectification at identified electrical synapses in the Drosophila giant fiber system. Curr Biol *18*, 1955-1960.

Phelan, P., Nakagawa, M., Wilkin, M.B., Moffat, K.G., O'Kane, C.J., Davies, J.A., and Bacon, J.P. (1996). Mutations in shaking-B prevent electrical synapse formation in the Drosophila giant fiber system. J Neurosci *16*, 1101-1113.

Pologruto, T.A., Sabatini, B.L., and Svoboda, K. (2003). ScanImage: flexible software for operating laser scanning microscopes. Biomed Eng Online *2*, 13.

Rayleigh, J.W.S. (1896). The Theory of Sound, Volume II.

Ritchie, M.G., Halsey, E.J., and Gleason, J.M. (1999). Drosophila song as a species-specific mating signal and the behavioural importance of Kyriacou & Hall cycles in D. melanogaster song. Animal Behaviour *58*, 649-657.

Ritchie MG, H.E., Gleason JM (1999). *Drosophila* song as a species-specific mating signal and the behavioural importance of Kyriacou & Hall cycles in *D. melanogaster* song. Anim Behav *58*, 649-657.

Robert, D., Miles, R.N., and Hoy, R.R. (1996). Directional hearing by mechanical coupling in the parasitoid fly Ormia ochracea. J Comp Physiol A *179*, 29-44.

Root, C.M., Semmelhack, J.L., Wong, A.M., Flores, J., and Wang, J.W. (2007). Propagation of olfactory information in Drosophila. Proceedings of the National Academy of Sciences *104*, 11826-11831.

Rosenmund, C., Stern-Bach, Y., and Stevens, C.F. (1998). The tetrameric structure of a glutamate receptor channel. Science *280*, 1596-1599.

Ruta, V., Datta, S.R., Vasconcelos, M.L., Freeland, J., Looger, L.L., and Axel, R. (2010). A dimorphic pheromone circuit in Drosophila from sensory input to descending output. Nature *468*, 686-690.

Rybak, F., Aubin, T., Moulin, B., and Jallon, J.-M. (2002a). Acoustic communication in Drosophila melanogaster courtship: Are pulse- and sine-song frequencies important for courtship success? Canadian Journal of Zoology *80*, 987.

Rybak, F., Sureau, G., and Aubin, T. (2002b). Functional coupling of acoustic and chemical signals in the courtship behaviour of the male Drosophila melanogaster. Proceedings of the Royal Society B: Biological Sciences *269*, 695-701.

Schilcher, F.V. (1976). The Role of Auditory Stimuli in the Courtship of *Drosophila Melanogaster*. Anim Behav *24*, 18-26.

Schneider, M., Barozzi, S., Testa, I., Faretta, M., and Diaspro, A. (2005). Two-photon activation and excitation properties of PA-GFP in the 720-920-nm region. Biophys J *89*, 1346-1352.

Sidi, S., Friedrich, R.W., and Nicolson, T. (2003). NompC TRP channel required for vertebrate sensory hair cell mechanotransduction. Science *301*, 96-99.

Sivan-Loukianova, E., and Eberl, D.F. (2005). Synaptic ultrastructure of Drosophila Johnston's organ axon terminals as revealed by an enhancer trap. J Comp Neurol *491*, 46-55.

Story, G.M., Peier, A.M., Reeve, A.J., Eid, S.R., Mosbacher, J., Hricik, T.R., Earley, T.J., Hergarden, A.C., Andersson, D.A., Hwang, S.W., *et al.* (2003). ANKTM1, a TRP-like channel expressed in nociceptive neurons, is activated by cold temperatures. Cell *112*, 819-829.

Strausfeld, N.J., and Bassemir, U.K. (1983). Cobalt-coupled neurons of a giant fibre system in Diptera. J Neurocytol *12*, 971-991.

Stretton, A.O., and Kravitz, E.A. (1968). Neuronal geometry: determination with a technique of intracellular dye injection. Science *162*, 132-134.

Sukharev, S.I., Blount, P., Martinac, B., Blattner, F.R., and Kung, C. (1994). A large-conductance mechanosensitive channel in E. coli encoded by mscL alone. Nature *368*, 265-268.

Tobin, D., Madsen, D., Kahn-Kirby, A., Peckol, E., Moulder, G., Barstead, R., Maricq, A., and Bargmann, C. (2002). Combinatorial expression of TRPV channel proteins defines their sensory functions and subcellular localization in C. elegans neurons. Neuron *35*, 307-318.

Tootoonian, S., Coen, P., Kawai, R., and Murthy, M. (2012). Neural representations of courtship song in the Drosophila brain. J Neurosci *32*, 787-798.

Tracey, W.D., Jr., Wilson, R.I., Laurent, G., and Benzer, S. (2003). painless, a Drosophila gene essential for nociception. Cell *113*, 261-273.

von Schilcher, F. (1976). The function of sine songs and pulse song in the courtship of *Drosophila melanogaster*. Animal Behavior *24*, 622 - 625.

Wang, Z., Singhvi, A., Kong, P., and Scott, K. (2004). Taste Representations in the Drosophila Brain. Cell *117*, 981-991.

Wilson, R.I., Turner, G.C., and Laurent, G. (2004a). Transformation of Olfactory Representations in the Drosophila Antennal Lobe. Science *303*, 366-370.

Wilson, R.I., Turner, G.C., and Laurent, G. (2004b). Transformation of olfactory representations in the Drosophila antennal lobe. Science *303*, 366-370.

Xiang, Y., Yuan, Q., Vogt, N., Looger, L.L., Jan, L.Y., and Jan, Y.N. (2010). Light-avoidance-mediating photoreceptors tile the Drosophila larval body wall. Nature *468*, 921-926.

Yorozu, S., Wong, A., Fischer, B.J., Dankert, H., Kernan, M.J., Kamikouchi, A., Ito, K., and Anderson, D.J. (2009). Distinct sensory representations of wind and near-field sound in the Drosophila brain. Nature *458*, 201-205.

Zhong, L., Hwang, R.Y., and Tracey, W.D. (2010). Pickpocket is a DEG/ENaC protein required for mechanical nociception in Drosophila larvae. Curr Biol *20*, 429-434.